Continuation of Microscopic and Microbial Insights into the Stony Coral Tissue Loss Disease (SCTLD) Outbreak Across Multiple Coral Species on Florida's Coral Reef

Florida Department of Environmental Protection
Coral Reef Conservation Program (CRCP) Project 11

Continuation of Microscopic and Microbial Insights into the Stony Coral Tissue Loss Disease (SCTLD) Outbreak Across Multiple Coral Species on Florida's Coral Reef

Final Report

Prepared By:
Jennifer L. Salerno PhD
Esther C. Peters PhD

George Mason University
Department of Environmental Science and Policy
4400 University Drive, MS 5F2
Fairfax, VA 22030-4444

June 30, 2021

Completed in Fulfillment of PO B859F1

Florida Department of Environmental Protection
Coral Reef Conservation Program
1277 N.E. 79th Street Causeway
Miami, FL 33138

This report should be cited as follows:
Salerno, J.L., and Peters, E.C. 2021. Continuation of Microscopic and Microbial Insights into the Stony Coral Tissue Loss Disease (SCTLD) Outbreak Across Multiple Coral Species on Florida's Coral Reef. Florida DEP. Miami, FL. Pp. 55.

This report was prepared for the Florida Department of Environmental Protection, Office of Resilience and Coastal Protection by George Mason University. Funding was provided by the Florida Department of Environmental Protection and the National Oceanic and Atmospheric Administration (NOAA) Coral Reef Conservation Program. The views, statements, findings, conclusions and recommendations expressed herein are those of the authors and do not necessarily reflect the views of the State of Florida, NOAA or any of its sub-agencies.

Cover Photo: Esther C. Peters

EXECUTIVE SUMMARY

Four integrated research tasks were performed using molecular biology, histology, and immunohistochemistry to provide insights into a possible mechanism of microbial infection that results in tissue loss, as well as potential pathogen(s) associated with stony coral tissue loss disease (SCTLD). For Task 1, molecular tools were used to characterize the endolithic communities of fungi, bacteria, and archaea from apparently healthy coral colonies, and affected and unaffected portions of diseased colonies sampled in 2016 and 2017. For Task 2, histological methods were used to characterize the endosymbiotic dinoflagellates in tissue from apparently healthy colonies and affected and unaffected portions of diseased colonies collected from Florida reefs or obtained following laboratory experiments conducted by Dr. Andrew Baker's research team at the University of Miami to examine their role in the pathogenesis of SCTLD. For Task 3, immunohistochemistry was used to investigate the role of programmed cell death (PCD) vs. necrosis in SCTLD. For Task 4, histoslides of apparently healthy and SCTLD-affected coral tissue samples were digitized using an Aperio ScanScope slide scanner. The resulting virtual microscopy files were uploaded with pertinent metadata on each sample to Florida's Fish and Wildlife Research Institute cloud storage. These virtual slides will be used for further study and interpretation by histopathologists considering the results of all SCTLD research.

Results from Task 1 indicated that the combination of proteinase K and lysozyme incubations, with an additional DNA cleanup step, did not increase PCR amplification efficiency of MCAV samples for bacterial/archaeal analysis as desired. However, these steps did increase the number of samples that amplified for fungal analyses. Preliminary analysis indicated that the endolithic coral microbiome (bacteria/archaea and fungi) varied in community composition based on host coral species and location, but not necessarily health state (with the caveat that diseased samples were limited in size for this analysis and additional analyses need to be performed to resolve fungal taxonomic identification). Additional bioinformatic analyses will be conducted to further investigate specific microbes driving observed differences and to examine the functional potential of the coral endolithic microbiome during different disease states. Results from Task 2 showed widespread necrosis and degradation within both SCTLD-exposed 'healthy' and 'lesion' samples. Lytic necrosis was seen in 45% of all histoslides examined (n=22), representing all five species of coral observed and all species of *Symbiodinium* (excluding *Cladocopium*). These results are consistent with what was seen in the 2016 FWRI samples in which zooxanthellae were often degraded or lysing in the apparently healthy, diseased, and unaffected tissue samples from all four species of coral. Lytic necrosis was observed in all species, with few to no zooxanthellae in these lesions that were usually restricted to the gastrodermis, and the mesoglea and epidermis remained intact. Gastrodermis adjacent to these lesions included pale-staining algal cells with vacuolation and swelling, then cell wall disintegration and lysing (ghosting). Results from Task 3 revealed that staining indicative of apoptosis was consistently observed in tissues of SCTLD-affected *Pseudodiploria strigosa, Montastraea cavernosa,* and *Orbicella faveolata*, indicating that this mode of cell death may be involved in SCTLD pathology. However, apoptosis was also observed in samples without an apparent lesion, indicating that

apoptosis may be an early indicator of disease before degradation can be detected morphologically, or may be normally expressed to some degree for routine epithelial cell replacement. In all species, staining for apoptosis was significantly more prevalent in diseased tissues, indicating that this process is increasingly expressed in disease, even if it is also part of healthy tissue functioning to a lesser degree. Histoslides were selected from 8 coral species examined by FWRI and scanned to capture the tissue section details digitally for Task 4. The image files have been uploaded and linked through a spreadsheet by filename to enable viewing of the slides from the Florida Fish and Wildlife Conservation Commission's website on SCTLD using Aperio's ImageScope software.

The results of this project contributed to a better understanding of disease mechanisms and insights on potential pathogenic agents involved in the progression of SCTLD in reef-building corals. Additional studies using these tools are needed to answer questions about the etiology and impact of SCTLD on Caribbean reefs.

ACKNOWLEDGEMENTS

The 2016 and 2017 frozen core samples and unstained histoslides cut from tissues embedded in paraffin blocks were provided by the Florida Fish and Wildlife Conservation Commission (FWC) Fish and Wildlife Research Institute (FWRI). We are grateful to Drs. Jan Landsberg and Yasu Kiryu, and Lindsay Huebner of FWRI, as well as Drs. Erinn Muller, Abigail Clark, and Katie Eaton of Mote Marine Laboratory, for coordinating shipping of the samples to us. Coral sample collections were made with funding support from the U.S. Fish and Wildlife Service through the State Wildlife Grants Program and the Florida Department of Environmental Protection's Coral Reef Conservation Program from the Southeast Florida Coral Reef Ecosystem Conservation Area and the Florida Keys National Marine Sanctuary. Andrew Baker and Caroline Dennison provided the samples from their laboratory experiments for Task 2. René Baumstark and Nick Alcaraz of the Coral Disease Response Data Management Team at FWRI, and Westley Farmer at FWC, developed procedures to archive the digitized slides for public access. Task Leaders for this project were Jordan Sims and Zachary Combs (George Mason University, GMU, Task 1), Samantha Cook (GMU, Task 2), Elizabeth McDonald (Nova Southeastern University, Task 3), and Cayla Williams (GMU, Task 4). They were assisted by Adam Murray and Liam Palmer (both at GMU).

TABLE OF CONTENTS

LIST OF FIGURES

LIST OF TABLES

LIST OF ACRONYMS AND ABBREVIATIONS

BBW	basal body wall
BLASTn	Basic Local Alignment Search Tool - nucleotide
CIBs	crystalline inclusion bodies
CITES	Convention on International Trade in Endangered Species
CNAT	*Colpophyllia natans*
COVID-19	coronavirus disease started in 2019 caused by the virus SARS-CoV-2
d	day(s)
DAB	diaminobenzidine
DEP	Florida Department of Environmental Protection
DLAB	*Diploria labyrinthiformis*
DNA	deoxyribonucleic acid
dUTP	2'-deoxyuridine 5'-triphosphate
FCR	Florida's Coral Reef
FISH	fluorescent in situ hybridization
FWC	Florida Fish and Wildlife Conservation Commission
FWRI	Florida's Fish and Wildlife Research Institute
GMU	George Mason University
g	gram(s)
H&E	hematoxylin and eosin
H_2O_2	hydrogen peroxide
h	hour(s)
HIER	heat-induced epitope retrieval
IHC	immunohistochemistry
ITS	internal transcribed spacer region
LCM	laser capture microdissection
LN	lytic necrosis
MCAV	*Montastraea cavernosa*
min	minute(s)
µL	microliter(s)
µM	micromolar
mL	milliliter(s)
MM	millimolar
MMEA	*Meandrina meandrites*
MML	Mote Marine Laboratory
NASA	National Aeronautics and Space Administration
NOAA	National Oceanic and Atmospheric Administration
NSU	Nova Southeastern University
OFAV	*Orbicella faveolata*
PAST	*Porites astreoides*
PBS	Phosphate-buffered saline
PCD	Programmed cell death
PCLI	*Pseudodiploria strigosa*
PIER	proteolytic-induced epitope retrieval

LIST OF ACRONYMS AND ABBREVIATIONS, CONTINUED

s	second(s)
SBW	surface body wall
SCTLD	stony coral tissue loss disease
SRA	Sequence Read Archive
SSID	*Siderastrea siderea*
SWG	State Wildlife Grant
RSMAS	Rosenstiel School of Marine and Atmospheric Science
TdT	terminal deoxynucleotidyl transferase
TUNEL	terminal deoxynucleotidyl transferase dUTP nick end labeling
URL	universal resource locator
WP	white plague

1. INTRODUCTION

Florida's Coral Reef (FCR) is currently experiencing a multi-year disease-related mortality event that has resulted in massive die-offs in multiple coral species (Precht et al. 2016, Walton et al. 2018). Over 21 species of coral, including both Endangered Species Act-listed and the primary reef-building species, have displayed tissue-loss lesions that often result in whole colony mortality. First observed near Virginia Key in late 2014, the disease has since spread to the northernmost extent of FCR, and south to the Marquesas in the Lower Florida Keys (Florida Department of Environmental Protection, https://floridadep.gov/rcp/coral/content/stony-coral-tissue-loss-disease-response), as well as to multiple distant sites in the northern Caribbean Sea (Atlantic and Gulf Rapid Reef Assessment, https://www.agrra.org/coral-disease-outbreak/).

Preliminary data presented during SCTLD Technical Workshops indicated that bacteria play a role in the disease process; however, the causative agent of the disease has not yet been identified and multiple factors may be involved. Under a previous award made by the Florida Department of Environmental Protection (DEP) (Coral Reef Conservation Program [CRCP] Project 11, PO B67289), our research group implemented an integrated and targeted approach to further investigate observations made by Drs. Jan Landsberg and Yasu Kiryu (Florida Fish and Wildlife Conservation Commission [FWC] and the Fish and Wildlife Research Institute [FWRI]) during their histopathological examinations of coral samples collected in 2016 and 2017, as well as some collected during the 2018 field surveys by FWRI. Their results indicated that focused studies of the roles played by zooxanthellae, apoptosis, and endolithic microorganisms in the pathogenesis of SCTLD were warranted.

The 2016–2017 samples are among the earliest collected for both histopathology and microbiology analyses, but with duplicate cores (comprised of coral skeleton, tissue, and mucous layer) collected for each sample type (healthy colonies and affected and unaffected portions of diseased colonies). One core was fixed in either formaldehyde or glutaraldehyde solution for light and transmission electron microscopy, respectively, and one was frozen for molecular studies of the microbiome. The biopsy cores from the 2016–2017 sampling effort were archived at -80 °C at FWRI. In 2018, a more extensive sampling effort was conducted by FWRI staff to obtain biopsy cores for histopathological examination, as well as surface mucus/tissue scrapings collected using a syringe technique for molecular microbiological analyses.

These samples became the focus of a study funded by a State Wildlife Grant (SWG) to Drs. Landsberg and Kiryu with Dr. Erinn Muller, Mote Marine Laboratory (MML), and Dr. Esther Peters, George Mason University (GMU). In addition to studying the samples for histopathological changes and microorganisms, genomic DNA from surface mucus/tissue samples was extracted by Drs. Muller and Abigail Clark at MML, processed, and sequenced to identify bacteria. In September 2019, Lindsay Huebner (FWRI), Dr. Muller, and Dr. Kim Ritchie (University of South Carolina at Beaufort) were awarded a U.S. Environmental Protection Agency grant to include the processing of the 2016–2017 frozen samples, replicating the method used on the 2018 field-collected syringe samples to collect surface mucus/tissue scrapings, extract the DNA, and sequence for microbial characterization (Bacteria and Archaea). These results will be compared with the histopathological results to help identify pathogenic microorganisms that may include the primary SCTLD-causing agent(s). The histopathology

samples embedded in paraffin blocks are archived by Drs. Landsberg and Kiryu at FWRI. They have provided additional unstained tissue sections mounted on glass microscope slides for fluorescent in situ hybridization (FISH) and laser capture microdissection (LCM) assays conducted in Dr. Peters' and Dr. Salerno's laboratories.

1.1. Proposed Research

Our interest in surveying the coral skeletal portions of the samples stemmed from observations that tissue damage and suspect bacteria or viruses (crystalline inclusion bodies, CIBs) have been found in the basal body wall of the coenenchyme and the polyp deep in the corallite, which may not be captured by surface scrapings (Figure 1). Three additional findings from the histopathological examinations performed by FWRI and GMU indicated that additional biotic or abiotic factors should also be considered in the pathogenesis of SCTLD. First, microscopic fungal hyphae that bore through the aragonite exoskeleton of the coral have been seen near the coral tissue in decalcified sections and are often associated with bacteria or archaea. This microbial consortium may release toxins that weaken the corals' immune responses or kill coral cells—alternatively, the degeneration of diseased coral tissue may alter the species in the endolithic community or their relative abundances. Second, the symbiotic dinoflagellates that live in the gastrodermal cells of the corals' polyps are degenerating some distance away from the tissue-loss margins, suggesting that they are more sensitive to a damaging factor than the corals' cells. Furthermore, genotype analyses of these algal cells from the coral species affected by the disease indicate that they largely belong to one genus, *Breviolum* (formerly Clade B). Are the algal cells involved in the coral tissue changes due to their susceptibility to biotic or abiotic pathogen(s) that reduce their ability to provide nutrients and waste recycling in the symbiosis? The third observation of note was that the affected corals variably displayed pathologic tissue changes that may be identified as necrosis (cell death) or apoptosis (programmed cell death, in which an enzyme cascade is triggered that destroys the cell and can be identified using immunohistochemical techniques). Understanding which of these changes is present (or whether both may occur in the same sample) can aid in our interpretation of the histopathological observations and pathogenesis related to potentially different etiological agents, or the disruption of the dinoflagellate symbiosis that is so important to the functioning of tropical reef-building coral species.

The overarching goal of this work was to investigate the roles of these three histopathological findings in the development of SCTLD. To date, most coral microbiome studies have employed molecular methods that used a homogenized slurry of coral mucus, tissue, and/or skeleton in varying combinations—providing information on the taxonomic composition of the whole microbial community—but resulting in the loss of spatial information with respect to the location of microbes on, or within, the coral host. Conversely, traditional histological techniques provided information on the tissue condition, inferred health state of the host, and location/presence of putative pathogens, but cannot confirm the taxonomic identification of microorganisms or identify other pathogens that may be involved. The information from both methods can be used to develop specific molecular probes to localize putative pathogens in the coral host's tissues.

Traditional histological techniques are also limited in that they allow for the diagnosis of cellular abnormalities based on morphological observations alone, which can miss the earliest stages of

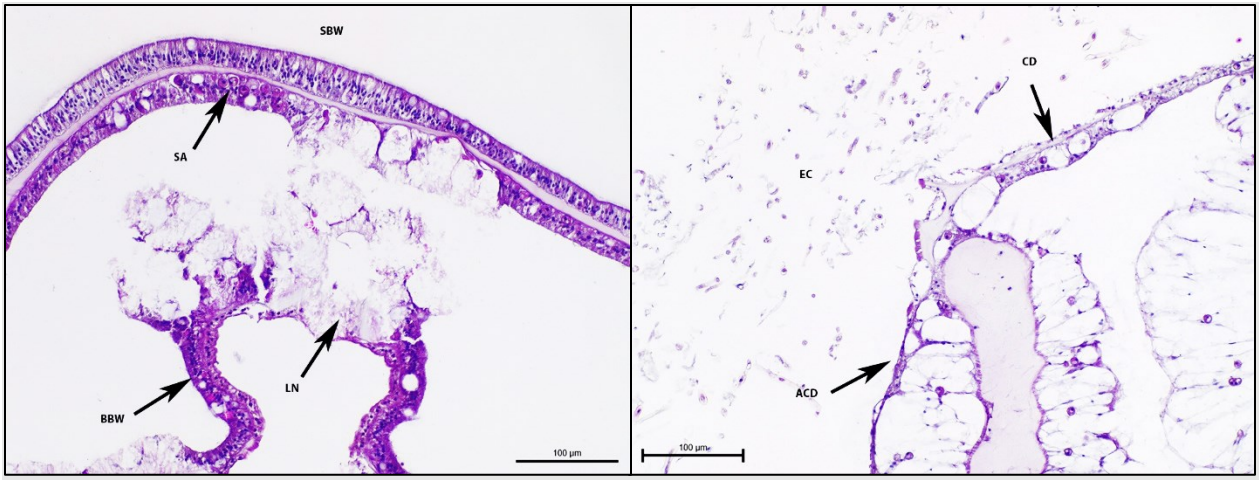

Figure 1: Histopathology observations in SCTLD. Left, middle right arrow lytic necrosis (LN) of the basal body wall (BBW) and surface body wall (SBW) gastrodermis in gastrovascular canal tissue covering the coenosteum in *Montastraea cavernosa* 107HD, 2016, Broward County 4, 20x, hematoxylin and eosin (H&E) staining. Upper arrow is pointing to degenerating symbiotic algae in surface body wall gastrodermis; lower left arrow is pointing to BBW where crystalline inclusion bodies and some suspect bacteria have been found. Right, endolithic community (EC) where the skeleton was removed adjacent to *Colpophyllia natans* tissue, 21U, 2016, Grecian Rocks, 20x, H&E. Note at upper arrow the calicodermis (CD) is sloughing, lower arrow points to atrophied or absent calicodermis (ACD).

malfunction before cells begin to degrade, causing a critical gap in spatial information regarding disease pathogenesis within the tissues. Conversely, immunohistochemistry (IHC) can target and highlight specific molecules within cells, providing sensitive and otherwise undetectable information about cell behavior before morphological changes. In the case of cell death, which is of particular interest in the SCTLD lesion of rapid tissue loss, IHC is a useful technique for distinguishing between necrosis and programmed cell death (PCD), which is difficult to identify by morphology alone. The TUNEL (terminal deoxynucleotidyl transferase dUTP nick-end labeling) technique enzymatically labels the free 3'-OH termini of fragmented single- and double-stranded DNA that occur during the early stages of PCD, allowing the visualization of apoptotic cells even before any morphological changes take place. Likewise, while histological observations can identify morphological changes within zooxanthellae, using sequencing data to identify dominant algal symbionts within diseased, unaffected, and healthy coral samples could provide evidence for species susceptibility. Alone, each of these methods present limitations and problematic data gaps, but when combined, provide a promising strategy to identify the causative agent(s) of SCTLD and to characterize the effects of the disease on the coral host.

1.2. Project Goals and Objectives

The outcomes of this project will be incorporated into the on-going coral disease response effort that seeks to improve understanding about the scale and severity of the FCR coral disease outbreak, identify primary and secondary causes, identify management actions to remediate disease impacts, restore affected resources and, ultimately, prevent future outbreaks. The project goals were to (1) use a combination of microscopy and molecular techniques to perform a

targeted characterization of the coral microbiome (dinoflagellate endosymbionts, fungi, bacteria, and archaea) in affected and unaffected portions of diseased colonies to document the effects of the disease on the coral microbiome and to potentially identify the causative agent(s) of stony coral tissue loss disease and (2) to investigate the role of programmed cell death (PCD) in SCTLD pathogenesis to determine whether this immune pathway is utilized by the coral host to respond to pathogens and ultimately contributes to the rapid tissue-loss lesion. Samples previously collected from numerous locations along FCR in 2016, 2017, and 2018 and processed for histology and genetic studies (extracted DNA) or stored frozen and available for additional molecular work were used. The histology samples collected by Dr. Andrew Baker's laboratory at the Rosenstiel School of Marine and Atmospheric Science, University of Miami following bleaching and dinoflagellate recolonization experiments to assess the role of the algal symbionts in the susceptibility of corals to SCTLD in South Florida (also funded by DEP) were included in the continuation of the project. Additional samples of freshly collected apparently healthy and diseased *Acropora cervicornis* were obtained from Nova Southeastern University's aquaculture facilities and fixed to test method adjustments to optimize the IHC procedure. Also, due to increasing interest among veterinary and invertebrate pathologists in the disease and the challenges of preparing and sharing glass histoslides, funding was provided to have selected histoslides digitally scanned and the files uploaded to FWRI's Azure cloud storage for downloading and viewing as if examining the tissue sections with a light microscope (virtual microscopy). The Methods and Results sections refer to the following tasks:

Task 1: Characterize the endolithic communities of fungi, bacteria, and archaea from apparently healthy coral colonies, and affected and unaffected portions of diseased colonies sampled in 2016 and 2017.

Task 2: Characterize the endosymbiotic dinoflagellates in mucus and tissue from apparently healthy and lesion samples and examine their role in the pathogenesis of SCTLD.

Task 3: Determine the role of programmed cell death vs. necrosis in SCTLD.

Task 4: Scan selected FWRI SCTLC project histoslides and upload to FWRI's cloud storage site.

2. METHODS

2.1. Task 1: Characterize the endolithic communities of fungi, bacteria, and archaea from apparently healthy coral colonies, and affected and unaffected portions of diseased colonies sampled in 2016 and 2017.

2.1.1 Sample Acquisition

Frozen core samples (51) from 2016 and 2017 were acquired from archived samples prepared by FWRI during their 2016–2018 sampling effort (Table 1). Samples were shipped frozen from MML in Sarasota, Florida, arriving at GMU's Potomac Environmental Research and Education Center, Woodbridge, Virginia, on March 18, 2020. Samples included apparently healthy, diseased, and unaffected tissues (Figure 2). Apparently healthy tissue was collected from coral

Table 1: Complete Task 1 bacterial/archaeal microbiome (not boldface) and fungal microbiome (boldface) sample list with numbers of samples per species, collection site, collection date, condition, and processing status (extracted, Extract.; sequenced, Seq.). D = Diseased, U = Unaffected, AH = Apparently Healthy.

Species	Collection Site	Collection Date	D	D	U	U	AH	AH
			Extract.	Seq.	Extract.	Seq.	Extract.	Seq.
CNAT	Grecian Rocks	2016	3 **3**	1 **3**	3 **3**	2 **3**	0 **0**	0 **0**
CNAT	Dustan Rocks	2017					3 **3**	2 **3**
DLAB	Grecian Rocks	2016	1 **1**	0 **1**	2 **2**	2 **2**	1 **1**	0 **1**
DLAB	Dustan Rocks	2017					5 **5**	3 **5**
PCLI	Martin County	2017					2 **2**	0 **1**
MCAV	Grecian Rocks	2016	1 **1**	0 **0**	2 **2**	0 **0**	1 **1**	0 **0**
MCAV	Martin County	2017					5 **5**	1 **1**
MCAV	Dustan Rocks	2017					3 **3**	0 **1**
OFAV	Dustan Rocks	2017					4 **4**	2 **4**
PAST	Martin County	2017					2 **2**	2 **2**
SSID	Martin County	2017					5 **5**	3 **4**
SSID	Dustan Rocks	2017					3 **3**	1 **3**
Totals	**All Sites**	**All Dates**	5 **5**	1 **4**	7 **7**	4 **5**	34 **34**	14 **25**

colonies showing no gross lesions. Diseased and unaffected tissues came from the same colony, with diseased coming from an area along a tissue-loss margin and unaffected from an area that was not grossly showing disease. Species included *Colpophyllia natans* (CNAT), *Diploria labyrinthiformis* (DLAB), *Montastraea cavernosa* (MCAV), *Porites astreoides* (PAST), *Pseudodiploria clivosa* (PCLI), *Orbicella faveolata* (OFAV), and *Siderastrea siderea* (SSID). Samples were obtained from one of three locations: Martin County, Grecian Rocks, or Dustan Rocks.

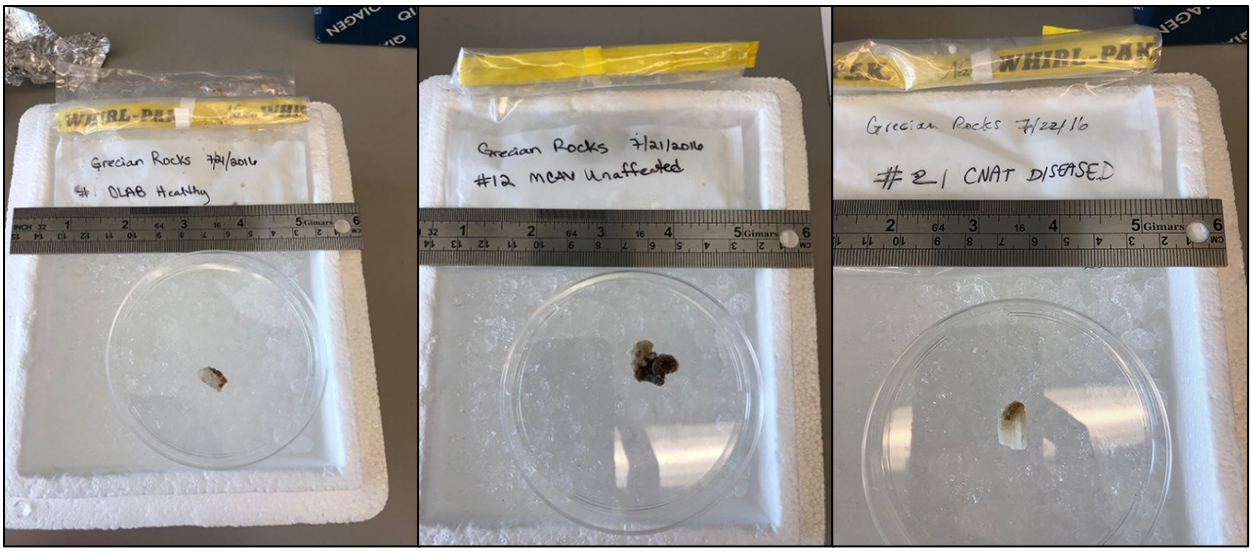

Figure 2: Examples of the frozen core samples used in this project.

2.1.2 DNA Extraction

Prior to processing, samples were photographed using an iPhone X (Apple, Inc.) for future reference. Samples were ground using sterile ceramic mortars and pestles. DNA was extracted using the DNeasy® PowerSoil® Kit (Qiagen) with the following modifications. Approximately 0.75 grams (g) of tissue from each sample was added to each Powerbead tube. Powerbead tubes were placed in an Omni Bead Ruptor 24 (Omni International, Inc.) for 45 seconds (s) rather than vortexing for 10 minutes (min). Samples were incubated with Proteinase K solution at 50 °C for 1 hour (h), followed by lysozyme at 37 °C for 1 h prior to extraction. DNA was eluted in 50 microliters (µL) of DEPC water and cleaned up using the DNeasy® PowerClean Pro Cleanup Kit (Qiagen) and stored at -80 °C until further analysis.

2.1.3 Polymerase Chain Reaction (PCR) Amplification of Bacterial, Archaeal, and Fungal Marker Genes

Prior to PCR amplification, extracted genomic DNA was quantified using a Qubit® 2.0 Fluorometer (Invitrogen Life Technologies) according to the manufacturer's protocol. All PCR reactions were carried out in duplicate. For 16s rRNA gene amplicon-based characterization, primers 515F (5'-GTG YCA GCM GCC GCG GTA A-3'; Parada et al. 2016) and 806R (5' GGA CTA CNV GGG TWT CTA AT-3'; Apprill et al. 2015) were used to target bacteria and archaea. A PCR master mix was prepared by adding the following per reaction: 5.9 µL of DEPC water, 2 µL of 10X PCR Gold Buffer (Applied Biosystems™ by Life Technologies™) for AmpliTaq Gold polymerase, 2 µL of 25 millimolar (mM) Mg mix and 2 µL of 0.1% bovine serum albumin (BSA), 0.1 µL of AmpliTaq Gold polymerase (5 units/µL), 2 µL of 2 mM each deoxynucleotide triphosphates (dNTPs), and 1 µL of both the forward and reverse primer in a 10 micromolar (µM) concentration. DNA amplification was performed in a 20 µl final volume solution per reaction, with 16 µL of master mix and 4 µl of extracted DNA from each sample aliquoted into 0.2-mL PCR tubes.

For fungal characterization, fungal-specific primers ITS1-F (5'CTT GGT CAT TTA GAG GAA GTA A-3'; Gardes and Bruns 1993) and ITS2 (5'- GCT GCG TTC TTC ATC GAT GC-3'; White et al. 1990) were used to amplify the internal transcribed spacer region 1 (ITS1) from extracted DNA. A PCR master mix was prepared by adding 7.9 µL of DEPC water, 2 µL of 10X PCR Gold Buffer (Applied Biosystems™ by Life Technologies™) for AmpliTaq Gold polymerase, 2 µL of 25 millimolar (mM) Mg mix, 2 µL of 2 mM each deoxynucleotide triphosphates (dNTPs), 1 µL of both the forward and reverse primer in a 10 micromolar (µM) concentration, 2 µL of 0.1% bovine serum albumin, and 0.1 µL AmpliTaq Gold polymerase (5 units/µL) per sample, to a 1.5-milliliter (mL) Eppendorf tube. DNA amplification was performed in a 20-µl final volume solution per reaction, with 18 µL of master mix and 2 µl of extracted DNA from each sample aliquoted into 0.2-mL PCR tubes.

All PCR amplifications were carried out on an Applied Biosystems® Veriti 96-well Thermal Cycler (Life Technologies, Frederick, MD). PCR conditions for 16s rRNA gene amplification were as follows: initial denaturation at 95 °C for 3 min; 30 cycles at 95 °C for 30 s, 65 °C for 60 s with each successive cycle reduced by 0.5 °C, and primer extension at 72 °C for 2 min; and 1 cycle of 95 °C for 30 s, 50 °C for 60 s, and 72 °C for 20 min. PCR conditions for ITS gene amplification were as follows: initial denaturation at 95 °C for 11 min; 35 cycles at 95 °C for 30 s, 50 °C for 30 s, 72 °C for 2 min +5 s per cycle; and 1 cycle of 72 °C for 30 min (White et al. 1990). PCR products were visualized on a 1% agarose gel with Invitrogen SYBR® Safe DNA gel stain and then stored frozen at -20 °C until further analysis.

2.1.4 Sequencing and Bioinformatic Analysis

All PCR products were cleaned using the QIAquick PCR Purification Kit (Qiagen) and quantified with the Qubit® 2.0 fluorometer, then approximately 500 nanograms (ng) of purified PCR product per sample was sent to the Genewiz® sequencing facility (South Plainfield, NJ) for amplicon sequencing on an Illumina MiSeq platform (Illumina Inc., San Diego, CA, USA). Due to methodological issues that prevented obtaining enough DNA for sequencing, approximately 50% of extracted samples were sent for sequence analysis. For metagenomic characterization, seven selected extracted cores from healthy colonies were chosen for sequencing (2 SSID colonies, 2 OFAV, 1 PAST, 1 MCAV, 1 CNAT). Approximately, 1350 ng of genomic DNA template per sample were sent to Genewiz® for sequencing on an Illumina NextSeq 550 platform (Illumina Inc., San Diego, CA, USA). Raw Fastq files were received from Genewiz® and amplicon sequences were analyzed using the QIIME2 bioinformatic pipeline (Version 2020.11). Amplicon sequences were demultiplexed and denoised, and paired-end reads were trimmed, checked for chimeras, grouped into amplicon sequence variants (ASV) using DADA2 (Callahan et al. 2016, Callahan et al. 2017), aligned with representative sequences using MAFFT (Katoh et al. 2002), and assigned taxonomy using the classify-consensus-vsearch option and the SILVA reference database (138 99% OTUs from 515F/806R) for 16S rRNA gene amplicons or a classifier trained on the UNITE reference database (sh_refs_qiime_ver8_dynamic_10.05.2021) for ITS gene amplicons. Beta diversity was calculated using Bray-Curtis dissimilarity (relative abundance of taxa) to compare differences across samples. Relative abundances of taxa were summarized across samples and displayed using bar plots.

2.2. Task 2: Characterize the endosymbiotic dinoflagellates in mucus and tissue from healthy, diseased, and unaffected portions of colonies and examine their role in the pathogenesis of SCTLD.

2.2.1. Summary of Completed Work

Task 2 is a direct continuation of the work funded under the FY20 Microscopic and Microbial Insights project. Previously, histological observations were undertaken systematically, beginning with examining dinoflagellate condition in the opportunistically collected 2016 field samples (processed by FWRI into histoslides that were sent to GMU) and moving towards the creation of new histoslides from recently collected coral cores that Dr. Andrew Baker's team at the University of Miami, Rosenstiel School of Marine and Atmospheric Sciences (RSMAS) collected and manipulated. This schedule was designed to build a foundation of knowledge so that similarities or differences could be more readily identified once the experiment samples became available. Results from the FWRI histoslide observations were presented in Salerno and Peters (2020). The Baker samples are also being analyzed using molecular techniques to confirm dinoflagellate classification and transcriptomics, which will then be complemented by the histopathological observations, allowing for more in-depth interpretation of what occurs in SCTLD pathogenesis.

2.2.2. Sample Acquisition

Core samples (92) were collected and fixed in aqueous buffered zinc formalin (1 part Z-Fix Concentrate diluted with 4 parts Instant Ocean® seawater 35 psu) during the FY20 DEP *Breviolum* project conducted by Dr. Andrew Baker's team at the Rosenstiel School of Marine and Atmospheric Sciences. The samples then arrived at the GMU Histology Laboratory on November 18, 2020. Task 2 was designed to complement Dr. Baker's project and provide histological observations for each phase of the experiment. This included unmanipulated control cores containing zooxanthellae with *Breviolum* as the dominant genus, bleached cores not exposed to SCTLD, bleached and then recovered cores containing *Durusdinium* not exposed to SCTLD, *Breviolum*-dominated cores exposed to SCTLD, bleached cores exposed to SCTLD, and bleached and then recovered cores containing *Durusdinium* exposed to SCTLD. Species included MMEA, PSTR, CNAT, OFAV, and DLAB. Unfortunately, samples were not able to be collected during each of the time points due to complications over the course of the experiment, including coral mortality following initial acclimation, poor shuffling of symbionts, slow recovery from initial bleaching resulting in partial mortality and poor health of the experimental cores, inconsistent bleaching and recovery times due to time constraints, and rapid mortality following initial SCTLD exposure. Of the 92 samples, 68 were collected before gross signs of SCTLD were observed (designated as H), and 24 were collected after gross lesions appeared (designated as L). Whole samples measured 1 inch in diameter, whereas half samples were cut down the middle. All samples were collected after exposure to SCTLD. No control samples were included due to limited amounts of remaining tissue. See Table 2 for a complete list of samples.

Table 2: FY20 DEP *Breviolum* project histology samples (H = apparently healthy, L = lesioned) by species of Symbiodiniaceae or bleached condition.

Species	*Breviolum*	*Cladocopium*	*Durusdinium*	*Bleached*	*, **	Total n
Healthy						
CNAT*	10			2	2	14
DLAB**			1	1	1	3
MMEA	7			1		8
PSTR	18		1	4		23
OFAV	4	5	4	6		19
Lesioned						
CNAT*	3		1	1		5
DLAB**			2			2
MMEA	2					2
PSTR				2		2
OFAV	3	6	4	1		14
Total	**47**	**11**	**13**	**18**	**3**	**92**

*Two additional CNAT samples with symbiont species unknown (n=19)
**One additional DLAB sample with symbiont species unknown (n=5)

2.2.3. Gross and Stereo Photography

Gross photos were taken of each sample using a Nikon CoolPix P7000 digital camera. A ruler was included for scale. The initial condition of each sample was observed including gross lesions, areas of tissue recession, algae overgrowth, and visible mesenteries to determine whether the sample should be enrobed in agarose. This was done to preserve tissue-loss margins, material that might be on the denuded skeleton, and possible microorganisms. Gross photos were also printed to record how the samples were trimmed into subsamples for processing.

Based on initial observations, each sample was also photographed using a stereo microscope for future reference. A Fisher Stereomaster microscope was used in conjunction with a smartphone to take photos at both 1x and 3x magnifications.

2.2.4. Enrobing, Decalcification, and Trimming

Of the 92 samples, 82 were enrobed in 2% low-melting point agarose. After being removed from the fixative, samples were washed for 30 min, then placed in a peelable mold, skeleton side down. The samples were then covered in 55–60 °C agarose and placed in a vacuum oven. Pressure was increased to 22 mm HG to ensure that the agarose infiltrated the skeleton, and all air bubbles were drawn out. Pressure was applied and released four times to ensure complete infiltration. The molds were cut away, excess agarose trimmed to leave about 2 mm around the tissue, and the sample was wrapped in lens paper before placing in a mega cassette to ensure the tissue stayed intact during decalcification. Non-enrobed samples were placed in tissue cassettes from the fixative solution and washed in tap water for 30 min. Because of the delicate nature of the coral tissue, decalcification was completed using chelation. Samples were immersed in 10% neutral pH ethylenediamine tetraacetic acid (EDTA). The solution was changed every three days

(d) and samples were checked regularly. Once the skeleton was completely gone, samples were washed using tap water for 30 min and then placed in 70% ethanol. This process took on average 1–2 months to complete.

Due to the small size of the samples as well as the thick skeleton, samples were trimmed after decalcification. Using the gross photos as a guide, each sample was trimmed into approximately 3 mm-wide strips. Orientation was considered, with most samples cut on the sagittal plane when possible so the surface body wall and coenenchyme down to the polyp bases would be visible in the histoslides. Consideration was also given to preserving tissue-loss margins, areas of tissue recession, and areas of algal overgrowth. Because the samples were so delicate, the trimmed strips were wrapped loosely in lens paper before placing them in the tissue cassette to ensure the tissue was not lost or re-oriented during processing. Each sample became 3–6 subsamples on trimming.

2.2.5. Processing, Embedding, Microtomy, and Staining

A Ventana Renaissance Tissue Processor 1530 was used following the schedules in Tables 3 and 4 to process all samples. After processing, samples were embedded in stainless-steel molds to form blocks using a Tanner Scientific TN1700 Embedding Center and ParaPro SEM Embedding Medium.

Blocks were sectioned 5 µm thick on an Olympus Cut 4060 Microtome. Three slides were created with two sections on each slide. Slide 1 was stained using Mayer's hematoxylin and eosin (Price & Peters, 2018). Slide 2 will be stained using Giemsa and Slide 3 will be used if additional stains are deemed necessary.

2.2.6. Slide Analysis

For this report, a general analysis of the coral tissue and endosymbiotic dinoflagellates was conducted. While originally planning to follow the same semi-quantitative analysis developed using the 2016 FWRI histoslides during the FY20 Microscopic and Microbial Insights project, from initial observations it was clear that the experiment samples displayed more varied microscopic degradation than was found in the prior histoslide analysis. To work in conjunction with the FY20 DEP *Breviolum* project, a broader analysis would need to be initially used, before specifically focusing on symbionts contained within gastrodermal tissue. Therefore, the following method was used for initial analysis.

A scoring system was used to rate both overall condition of the tissue and severity of degradation in specific areas of the tissue. All observations were done under 10x magnification. Photomicrographs were taken using an Olympus BX43 Clinical Microscope with an attached Olympus DP72 camera using CellSens software. Scoring for overall condition was as follows: excellent (0), very good (1), good (2), fair (3), poor (4), and very poor (5). Excellent tissue showed no signs of degradation or necrosis. Very good tissue showed no signs of degradation or necrosis but some mechanical damage caused by collection/coring might be visible on the epidermis of septa or along edges of tissue. Good tissue showed mild signs of degradation that could include abnormal Symbiodiniaceae (atrophy, swelling, enlargement or vacuolization of the

Table 3: Enrobed coral tissue processing program

Time	Solution	Vacuum	Temperature
30 min	70 % Ethanol		
30 min	70% Ethanol		
30 min	80% Ethanol		
45min	95% Ethanol		
30 min	Reagent Alcohol		
30 min	Reagent Alcohol		
45min	Reagent Alcohol		
45min	Clearify	15 mm Hg	
30 min	Clearify		
45min	Clearify	15 mm Hg	
45min	Paraffin Plus		60° C
45min	Paraffin		60° C
45min	Paraffin	15 mm Hg	60° C

Table 4: Standard coral tissue processing program

Time	Solution	Vacuum	Temperature
30 min	70 % Ethanol		
30 min	70% Ethanol		
15 min	80% Ethanol		
15 min	95% Ethanol		
15 min	Reagent Alcohol		
15 min	Reagent Alcohol		
15 min	Reagent Alcohol		
15 min	Clearify		
15 min	Clearify		
15 min	Clearify		
30 min	Paraffin Plus		60 °C
15 min	Paraffin		60 °C
15 min	Paraffin	15 mm Hg	60 °C

symbiosome, or lysing/ghosting), abnormal mucocytes in the epidermis or mesenterial filaments (atrophy, hypertrophy, or necrosis), abnormalities within the calicodermis (atrophy, sloughing, or hyalinization), and abnormalities within the cnidoglandular bands (vacuolization, atrophy, or necrosis). Fair tissue showed moderate signs as outlined above. Poor tissue showed marked signs as listed above. Very poor tissue showed severe signs as listed above. Note that the first observations done using this method were qualitative and subjective in nature.

2.3. Task 3: Determine the role of programmed cell death vs. necrosis in SCTLD

This task built on the previous work to identify areas of PCD in SCTLD-affected coral tissues by further optimizing techniques for cell death analysis on formalin-fixed paraffin-embedded

(FFPE) coral tissues, and by applying that resulting protocol to coral tissue histoslides to visualize the role of PCD in the SCTLD lesions of three target species: *Pseudodiploria strigosa*, *Obicella faveolata*, and *Montastrea cavernosa*. The TUNEL staining technique was further refined for use on FFPE coral tissues by optimizing the protocol on apparently healthy and diseased *Acropora cervicornis* samples collected in August 2020. The optimized protocol was then applied to tissue cores from three SCTLD-affected colonies and three healthy colonies of each target species listed above to determine the cell death pathology in these samples.

2.3.1. Sample Acquisition

Fragmented branches of apparently healthy (n=12) and diseased (white-band disease/rapid tissue loss) (n=20) *Acropora cervicornis* were collected from Nova Southeastern University's (NSU) aquaculture facilities (Marine Larval Ecology Laboratory land-based nursery; Coral Reef Restoration and Monitoring Laboratory offshore nursery) for use in the TUNEL methods development portion of this task (Table 5). This species was used as a model organism for the development of this protocol due to its high abundance and accessibility in coral nurseries and because the histology of this species has been well studied by Dr. Peters and former students and colleagues at GMU and NSU. Clipped branches were immediately fixed in either a solution of 1 part Z-Fix Concentrate (Anatech, Ltd.) diluted with 4 parts filtered seawater (n=15) or 4% paraformaldehyde (PFA) in phosphate buffered saline (PBS) (n=17) and transported to the NSU Oceanographic Center laboratories in a dark cooler. Samples fixed in the Z-Fix solution were fixed for ~18–23 d and samples in 4% PFA were fixed for ~20 h before being stop-fixed in 70% ethanol prior to further processing. Samples exhibiting severely necrotic lesions were enrobed in agarose to maintain tissue integrity during further processing.

Tissue sections of SCTLD lesions were prepared from the tissue-core samples archived at FWRI and collected during the 2016–2018 sampling effort (Table 6). Diseased tissue cores were taken from the active tissue-loss margins of corals with SCTLD, unaffected tissue cores were taken from the apparently healthy portions of a colony with an active SCTLD lesion, and apparently healthy tissue cores were taken from corals with no visible signs of tissue loss. Samples were immediately fixed in a solution of 1 part Z-Fix Concentrate (Anatech, Ltd.) diluted with 4 parts filtered seawater and transported to FWRI in a dark cooler. Samples were fixed for 100–256 d before being stop-fixed in 70% ethanol prior to further processing. Samples exhibiting severely necrotic lesions were enrobed in agarose to maintain tissue integrity during further processing.

2.3.2. Sample Processing for Histology and Immunohistochemistry

All *A. cervicornis* samples were decalcified in 10% EDTA and then embedded in paraffin blocks in the NSU Histology Laboratory to obtain sections mounted on glass slides. Serial tissue sections were taken from each block, half to be stained with Mayer's hematoxylin and eosin for general tissue structure, and half to be stained using immunohistochemical techniques for apoptosis.

The Apoptag *in situ* Apoptosis Detection Kit (Millipore Sigma) was used to highlight areas of apoptosis in paraffin-embedded coral tissues, which uses the TUNEL method (terminal deoxynucleotidyl transferase dUTP nick-end labeling) to stain the fragmented DNA ends

Table 5: Task 3 sample list of white-band disease- (WBD) and rapid tissue loss (RTL)-affected fragments of *A. cervicornis* used for TUNEL method optimization

Species	Fixative Type	Fixative Duration	Diseased	Unaffected	Apparently Healthy
ACER	Z-Fix:seawater	18–23 d	10	0	5
ACER	4% PFA	20 h	10	9	7
Total			**20**	**9**	**12**

Table 6: Task 3 sample list of SCTLD-affected tissue samples acquired from FWRI archive

Species	Collection Sites	Collect-ion Date	Fixative Type	Fixative Dura-tion	Disease	Unaffected	Apparent-ly Healthy
PSTR	West Turtle Shoal, NSP, Dustan Rocks, East Turtle Shoal	2018	Z-Fix: seawater	104–256	3	3	3
MCAV	West Turtle Shoal, NSP, Dustan Rocks, East Turtle Shoal	2018	Z-Fix: seawater	100–302	3	3	3
OFAV	West Turtle Shoal, NSP, Dustan Rocks, East Turtle Shoal	2018	Z-Fix: seawater	102–256	3	3	3
Total					**9**	**9**	**9**

associated with this process. Tissue sections were first dewaxed in xylene and rehydrated in a series of alcohols before being treated for epitope retrieval, which breaks the protein crosslinks that are formed during fixation to expose the antigens that will facilitate DNA labelling. After treatment for epitope retrieval (incubation in 5µg/mL proteinase K for 5 min), sections were washed in phosphate-buffered saline (PBS) and incubated with an equilibration buffer before

incubation with dUTP-digoxigenin with terminal deoxynucleotidyl transferase (TdT enzyme) in a humidified chamber for 1 h at 37 °C. The reaction was stopped in stop wash buffer and tissue sections were washed in PBS before incubation with an anti-digoxigenin antibody that is conjugated to a peroxidase reporter molecule in a humidified chamber for 30 min. This antibody conjugate binds to the fragmented DNA strands that were labelled during incubation with TdT enzyme and reacts with a peroxidase substrate to create the orange-brown staining indicative of apoptosis. After the incubation step with diaminobenzidine (DAB) peroxidase substrate, the slides were washed and counterstained with Mayer's hematoxylin to allow observation of intact nuclei alongside apoptotic nuclei. Slides were then washed and cleared with n-butanol and xylene before applying the coverslip with Permount mounting medium.

Through a series of TUNEL optimization experiments, the following steps of the Apoptag protocol were customized for use on FFPE coral tissues:

- The **addition of a blocking step to reduce the amount of non-specific antibody binding** to tissues. After the incubation period with TdT enzyme and Reaction Buffer, a 30-min incubation step with Roche blocking reagent was added before incubation with the anti-digoxigenenin conjugate.

- **The concentration of proteinase K**, the digestive enzyme used to expose antigens that are masked by the protein crosslinking that form during fixation, was reduced to a concentration of **5 µg/mL proteinase K for an incubation of 5 min.**

- The **incubation time with diaminobenzidine (DAB) peroxidase substrate** was reduced from the manufacturer recommended duration of 1–5 min to ~30 s to reduce excessive background staining.

- The **incubation time in hydrogen peroxide (H_2O_2)**, which is intended to quench endogenous peroxidases that interfere with specific DAB-staining of nuclei, was increased from the manufacturer's recommended duration of 5 min to 30 min.

2.3.3. Slide Reading for Histopathology and Cell Death

Photomicrographs of tissue sections were taken at 400x magnification at ten random locations along the surface body wall (SBW) and basal body wall (BBW), and five random locations along both mesenteries and cnidoglandular bands (CGB) for a total of 30 photomicrographs per section. The high number of replicates within each sample was chosen to reduce the influence of biases towards areas of high- or low-positive staining with DAB and to capture a comprehensive representation of sample-wide patterns of cell death. To quantify the degree of positive staining with DAB substrate, indicating DNA-fragmentation associated with apoptosis, all photomicrographs were analyzed using the following batch image manipulation and analysis pipeline of ImageJ Fji 2 plugin photo analysis software and Photoshop (Figure 3). First, a color deconvolution filter was applied to images using the H & DAB channels to separate the image into its blue and orange parts, thereby separating all tissues stained with DAB (orange) and those stained with hematoxylin (blue) into separate files for all further processing steps using the Fiji2 plugin of ImageJ software. To remove influence from background staining and to isolate the

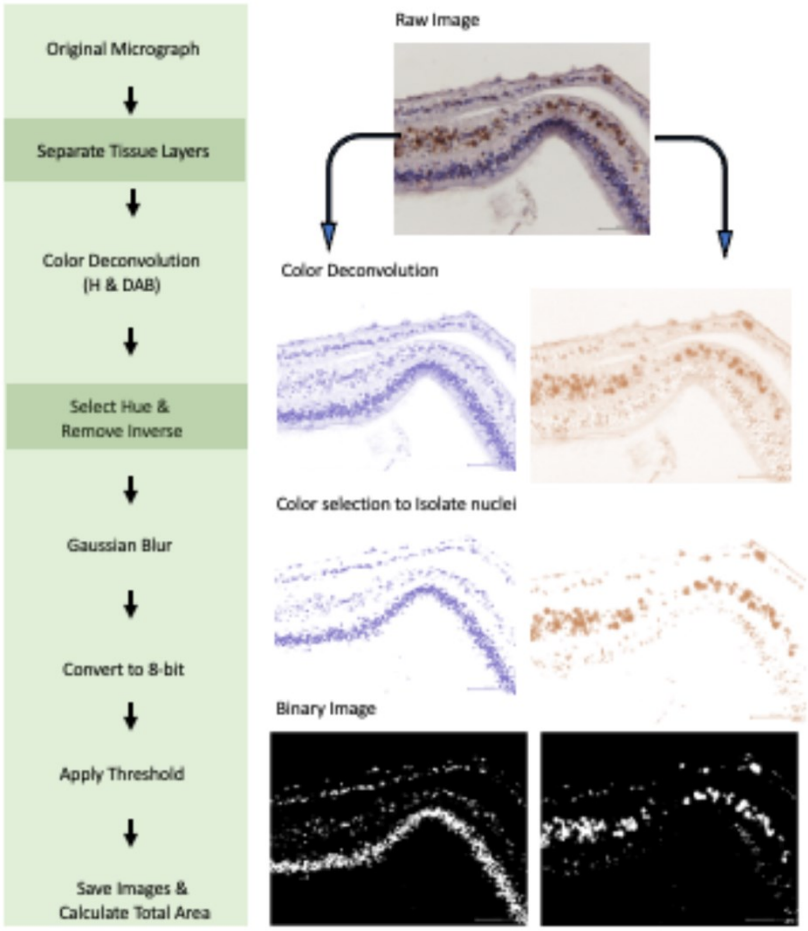

Figure 3: Image analysis pipeline to calculate total stained area using Photoshop and ImageJ (Fiji2) software. Image-processing steps in dark green box were completed in Photoshop, steps in lighter green box were completed in ImageJ.

staining of nuclei only, the Photoshop Color Select tool was used to select the darkest hue of the photomicrograph and remove the inverse selection, leaving only the darkest-staining areas (nuclei) in each micrograph for further analysis. A Gaussian Blur (Sigma: 2.00) was then applied to the selection to reduce pixel noise. The image was then converted to an 8-bit gray-scale image and a threshold was applied to create a binary image with all objects (stained nuclei as isolated from prior steps) appearing as white against a black background. The extent of PCD and spatial patterns of cell death within tissues was determined by quantifying the area of white in each image. The labeling index was calculated by dividing the area of DAB-stained material by the total area of stained material for each micrograph. This was chosen as the metric for PCD prevalence rather than positive and negative cell counts due to the high overlap of nuclei in dense tissue layers (epidermis, cnidoglandular bands) and insufficient segmenting techniques using ImageJ Software.

To determine any relationships between other histological markers of SCTLD microscopic lesions and prominence of cell death activity, the following eleven pathological parameters were scored for presence (1)/absence (0) in 5 randomly-selected photomicrographs of each tissue layer

per sample (n=15/sample): vacuolization, tissue-layer rupture, tissue-layer dissociation, necrosis, BBW swelling, mucocyte hypertrophy, zooxanthellae vacuolization, zooxanthellae necrosis, angular nuclei of zooxanthellae, nuclear blebbing, and subepidermal vacuoles.

2.4. Task 4: Scan Selected FWRI SCTLD Project Histoslides and Upload to FWRI's Cloud Storage Site

2.4.1. Sample Acquisition

Samples of several coral species were collected from 13 sites along the Florida Reef Tract between 2015 and 2018 for histopathological examination (Landsberg et al. 2020). These species included *M. cavernosa, O. faveolata, S. siderea, C. natans, D. labyrinthiformis, P. clivosa, Porites astreoides, Dendrogyra cylindrus,* and *Meandrina meandrites*. SCTLD was established at these sites. Reference samples from seemingly healthy corals without tissue loss or discoloration were collected in Martin County and the Middle Keys in 2017. Additional reference samples were collected from the Lower Keys and offshore Key West in 2018. Samples of *Eusmilia fastigiata, P. strigosa,* and *M. cavernosa* were collected from these sites between August and October 2015.

2.4.2. Sample Processing for Histology and Histopathology

All samples were collected by biopsy. For healthy corals (histology healthy, HH), a single 2.5-cm diameter circular core of tissue and skeleton was collected. For diseased corals, cores were collected from unaffected tissue (histology unaffected, HU) and at the margin between skeleton and intact tissues (histology diseased, HD). Samples for histology were preserved in a solution of 1 part Z-fix and 4 parts 0.2 µm-filtered natural seawater (or 35 salinity artificial seawater). All processing and histology were done at FWRI, St. Petersburg, Florida. Those with obvious lesions were examined under higher magnification and photomicrographs were taken. HD samples were enrobed with 1.5% agarose in a heated vacuum oven following decalcification with 10% EDTA to preserve surface organisms. The samples were then trimmed, embedded in paraffin or glycol methacrylate plastic resin (JB4), and stained with Mayer's hematoxylin and eosin. Special stains were performed on additional sections from each block, including alcian blue, Fontana-Masson, Grocott's methenamine-silver nitrate, Giemsa, Macchiavello, methyl green pyronin, periodic acid-Schiff reagent with metanil yellow, and thionin (Landsberg et al. 2020).

2.4.3. Histoslide Selection and Quality Assurance

Three hundred histoslides prepared from these samples were selected for the histoslide scanning project. GMU and Dr. Yasu Kiryu (FWRI) collaborated with the Disease Advisory Committee's Histopathology Core Research Group to provide these histoslides (GMU had previously received histoslides from some of these samples). Each histoslide was tracked using an Excel spreadsheet prepared in 2015 for SCTLD sample collection. This spreadsheet was revised for the purposes of this task. The Excel spreadsheet listed samples using their unique IDs, as well as the number and types (embedding medium and staining) of slides associated with them. Filenames were developed for each histoslide to include ID, species,

processing, and staining. Other identifying characteristics such as species, date of collection, and location of collection were documented.

2.4.4. Histoslide Scanning and Cloud Storage

The histoslides were securely packaged and delivered to ResourcePath LLC in Sterling, Virginia. Each histoslide was scanned at 40x magnification using an Aperio ScanScope slide scanner to produce high-resolution digitized images. Image files were stored on 2 TB external hard drives due to their large file size. The hard drives were sent to Westley Farmer at FWC, Tallahassee, Florida, so the image files could be uploaded to FWC's Microsoft Azure cloud. The revised final spreadsheet was sent to Dr. René Baumstark, FWRI Information Science and Management, along with text explaining the project, how the histoslides were prepared, and draft instructions on how to access the histoslides to be posted on their website.

3. RESULTS

3.1. Task 1

The DNA concentrations of extracted samples ranged from 293 ng/mL to >100,000 ng/mL. The average concentration across all samples was 12,222.2 ng/mL (n=46). Extracted DNA from the apparently diseased samples ranged in concentration from 293 ng/mL to 1,550 ng/mL with a mean concentration of 660.5 ng/mL (n=5). Extracted DNA from the apparently healthy samples ranged in concentration from 400 ng/mL to >100,000 ng/mL with a mean concentration of 12,763.8 ng/mL (n=34). Extracted DNA from the unaffected areas of apparently diseased samples ranged in concentration from 502 ng/mL to 2,670 ng/mL with a mean concentration of 993.9 ng/mL (n=7). PCLI samples had an average concentration of 1,134.2 ng/mL (n=2). MCAV samples had an average concentration of 12,222.2 ng/mL (n=12). DLAB samples had an average concentration of 5,400.8 ng/mL (n=9). CNAT samples had an average concentration of 9,484.2 ng/mL (n=9). SSID samples had an average concentration of 13,021.6 ng/mL (n=8). OFAV samples had an average concentration of 16,755.7 ng/mL (n=4). PAST samples had an average DNA concentration of 20,488.9 ng/mL (n=2).

3.1.1. Polymerase Chain Reaction (PCR) Amplification of Bacterial, Archaeal, and Fungal Marker Genes

Nineteen of 46 processed and extracted samples (41%) were successfully PCR-amplified using bacterial/archaeal-specific primers. These included 5/9 processed CNAT samples (55.6%), 2/2 processed PAST samples (100%), 4/8 processed SSID samples (50%), 2/4 processed OFAV samples (50%), 5/9 processed DLAB samples (55.6%), and 1/12 processed MCAV samples (8.3%). No PCLI samples were successfully amplified 0/2 (0%). Thirty-four of 46 processed and extracted samples (73.9%) were successfully PCR-amplified using fungal-specific primers. These included 9/9 processed CNAT samples (100%), 2/2 processed PAST samples (100%), 7/8 processed SSID samples (87.5), 4/4processed OFAV samples (100%), 9/9processed DLAB samples (100%), 2/12 processed MCAV samples (16.7%), and 1/2 PCLI samples.

3.1.2. Microbiome Composition Based on Sequencing and Bioinformatic Analysis

For 16S rRNA gene amplicons, a total of 4.4 million sequences were retrieved, with an average of 222,192 sequences per sample prior to quality filtering, denoising, merging, and chimera removal. A total of 3.3 million sequences, with an average of 167,353 sequences per sample remained after these processes. Reads identified as chloroplast or mitochondrial DNA were removed, leaving 2,826,987 reads representing 28,792 ASVs for analysis. Preliminary results from principal coordinates analysis (PCoA) based on Bray-Curtis distances did not reveal any clear clustering based on species, health state, or location (Figure 4). However, PERMANOVA analysis revealed differences between Martin County and the other two reef sites ($p=0.001$) as well as species differences ($p=0.002$) between CNAT and SSID ($p=0.009$) and DLAB and SSID ($p=0.035$). No differences were observed by health state ($p=0.505$). At the class level, Gammaproteobacteria, Alphaproteobacteria, and Planctomycetes were present in all coral samples (Figure 5 and Table 7). Classes Bacteroidiia and Clostridia were present in varying abundances in nearly all samples with no discernable pattern among species or health state. In the single diseased CNAT sample, Order Rhizobiales, Genus *Halanaerobium*, Genus *Psychrobacter*, Class Rhizobiaceae, genera *Roseitalea* and *Mesorhizobium*, Genus TSAC18 (uncultured Clostridia) were all present.

For ITS gene amplicons, a total of 7.1 million sequences were retrieved, with an average of 203,799 sequences per sample prior to quality filtering, denoising, merging, and chimera removal. A total of 5.2 million sequences, with an average of 138,340 sequences per sample remained after these processes. Preliminary results from PCoA based on Bray-Curtis distances revealed that some samples clustered based on species and location (Figure 6). In particular, CNAT and DLAB samples clustered together. PERMANOVA analysis revealed differences between Grecian Rocks and the other two reef sites ($p=0.001$), and species ($p=0.001$), but not health state ($p=0.247$). A preliminary examination of the relative abundance of taxa across samples reveals a high presence of unidentified fungi (Figure 7 and Table 8). Other bioinformatic approaches and reference databases will be explored to resolve taxonomy.

All raw sequence data from these samples will be publicly available through NCBI's Sequence Read Archive (SRA) database upon publication or by request. The 16S rRNA gene amplicon sequences will be made available to the Disease Advisory Committee for inclusion in a meta-analysis being performed by a working group within the Pathogen ID/Microbiome SubTeam.

3.2. Task 2

Most of this research period was devoted to sample preparation. As described in the methods section, chelation was used during decalcification. This process took approximately 1–2 months to complete per sample. 277 paraffin blocks have been created so far and 95 samples have H&E histoslides prepared. 285 sections have been cut including the duplicates for Giemsa staining and the additional serial slide for other stains if deemed necessary in the future. Slides are being created as the samples are processed. The 22 slides chosen to be analyzed were done so at random by species. Because of this there are a limited number of L slides (n=3). This is also due to the higher number of apparently healthy samples, as well as the fact that most L samples consist of OFAV (n=14/25), which typically take longer to decalcify.

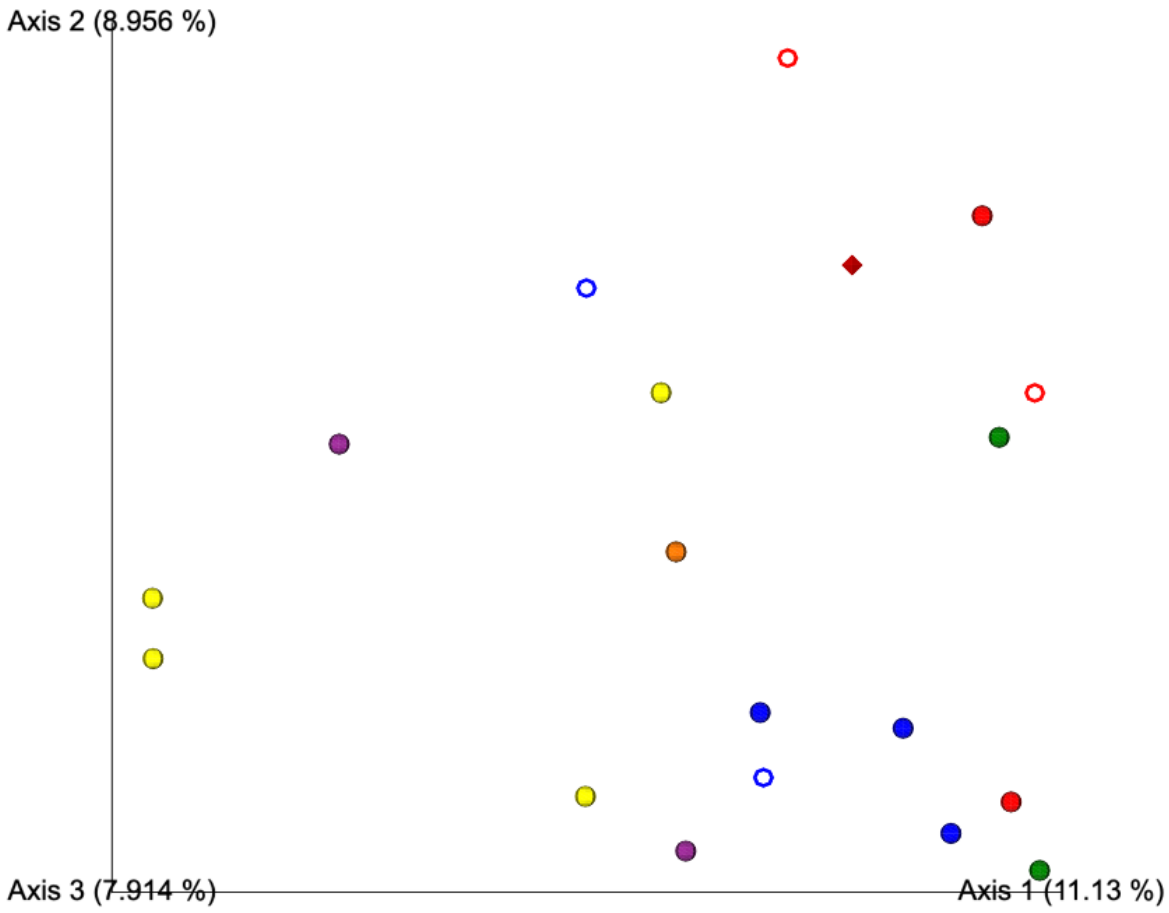

Figure 4: Principal coordinates analysis (PCoA) based on Bray-Curtis distances for 16S rRNA gene amplicon sequences. Points that are closer together are more similar in microbial community composition and those that are further apart are more dissimilar. Red points = CNAT, dark blue = DLAB, orange = MCAV, purple = OFAV, and yellow = PAST. Spheres =

3.2.1. Initial Histoslide Analysis

Initial results from the histoslide examinations showed widespread necrosis and degradation throughout the entirety of the tissue (Table 9). All samples were collected after exposure to SCTLD, and lytic necrosis (LN) is visible in 10 of the 22 slides examined (45%). On initial observations, it did not seem as though LN was more prevalent in any one coral species or in the presence of any one dinoflagellate type, but sample size was small.

Lytic necrosis was seen in all five of the coral species and across all species of *Symbiodinium* except for *Cladocopium* in an OFAV sample; however, this was likely due to the poor health of that single sample overall, which displayed extensive necrosis. In some cases, the gastrodermis

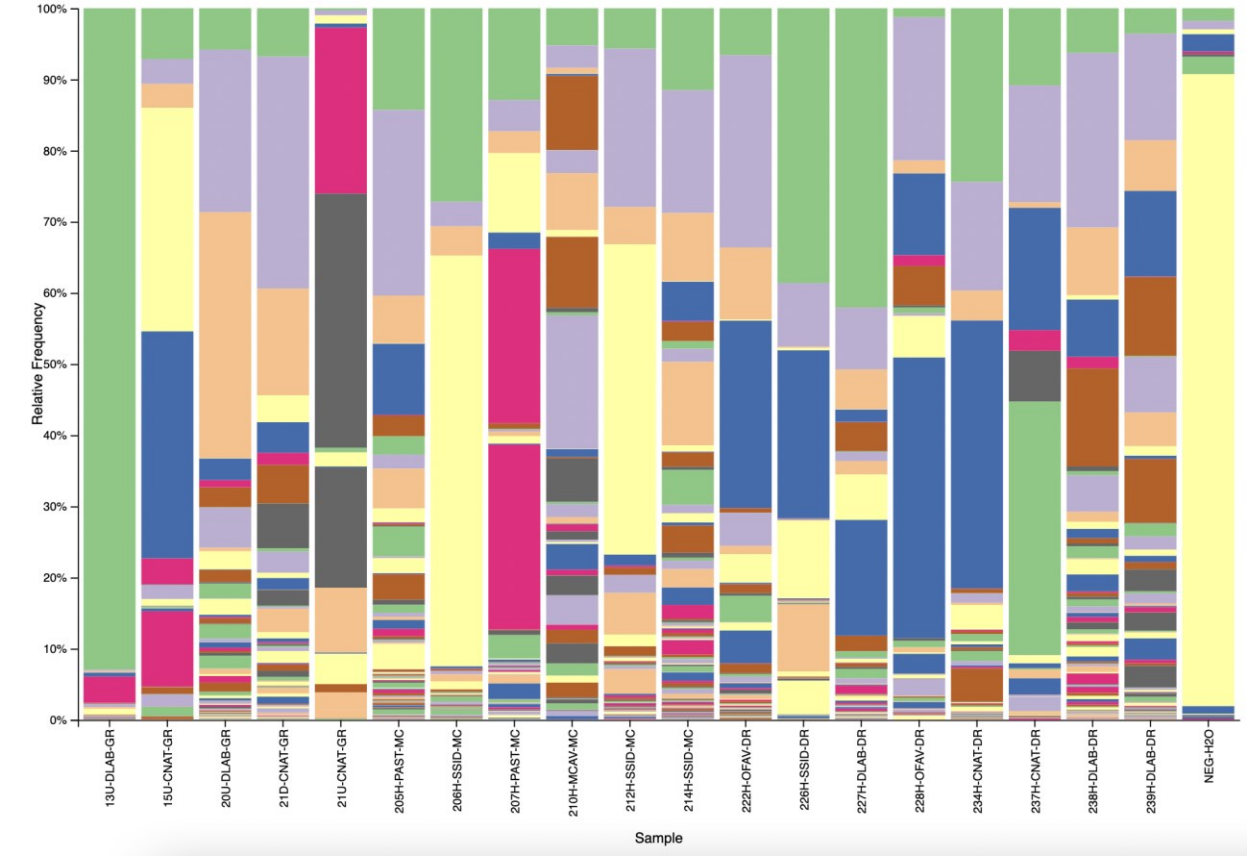

Figure 5: Taxonomic bar plot summary for 16S rRNA gene amplicon sequences (class level). The x-axis contains sample IDs: sample number, health state (H = apparently healthy, U = unaffected, D = diseased), coral species, location collected. The y-axis is the relative abundance of different taxa in each sample. A kit blank was also included for comparison. Color codes for taxonomic groups are indicated in the legend on the following page (Table 7).

Table 7: Color codes for the taxonomic groups in Figure 5

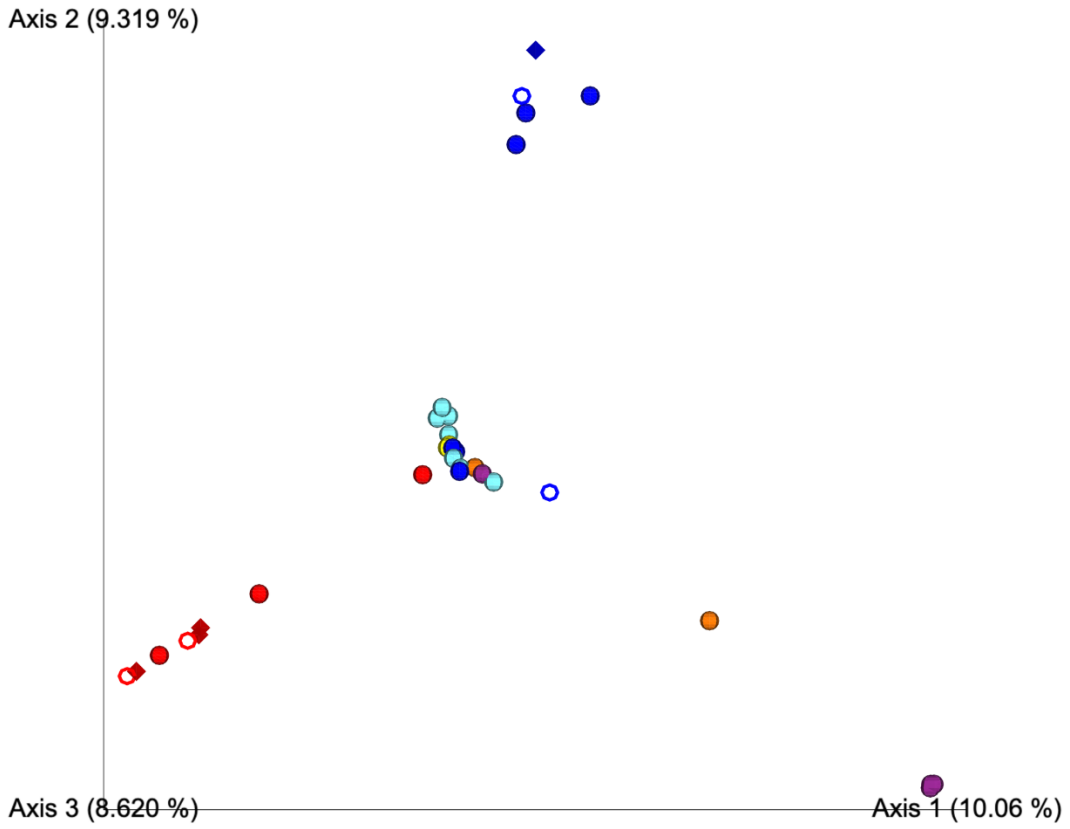

Figure 6: Principal coordinates analysis (PCoA) plot based on Bray-Curtis distances for ITS gene amplicon sequences. Points that are closer together are more similar in fungal community composition and those that are further apart are more dissimilar. Red points = CNAT, dark blue = DLAB, orange = MCAV, purple = OFAV, yellow = PAST, and light blue = SSID. Spheres = healthy, rings = unaffected, diamonds = diseased, stars = PCR positive.

of the SBW detached from mesoglea either partially or completely. Areas of LN were isolated with surrounding tissue showing signs of degradation, including vacuolation and lysing, with the algal cells appearing pale as staining quality decreased and the cell wall disintegrated (ghosting) (Figure 8, photomicrograph 4). LN was also present in 2 of the 6 bleached slides examined, despite the absence of symbionts (Figure 9, photomicrographs 3 and 4).

3.2.2. Further Processing and Histopathological Examination

While signs of SCTLD were present (LN, vacuolization in the SBW, and degradation of symbionts), the tissue also displayed more general forms of necrosis. When first observing the samples grossly, algal overgrowth and corresponding tissue recession, denuded skeleton, and released mesenteries were present in 82 of the 92 samples, prompting them to be enrobed to help ensure the integrity of the tissue during processing. These included all 23 of the lesioned samples

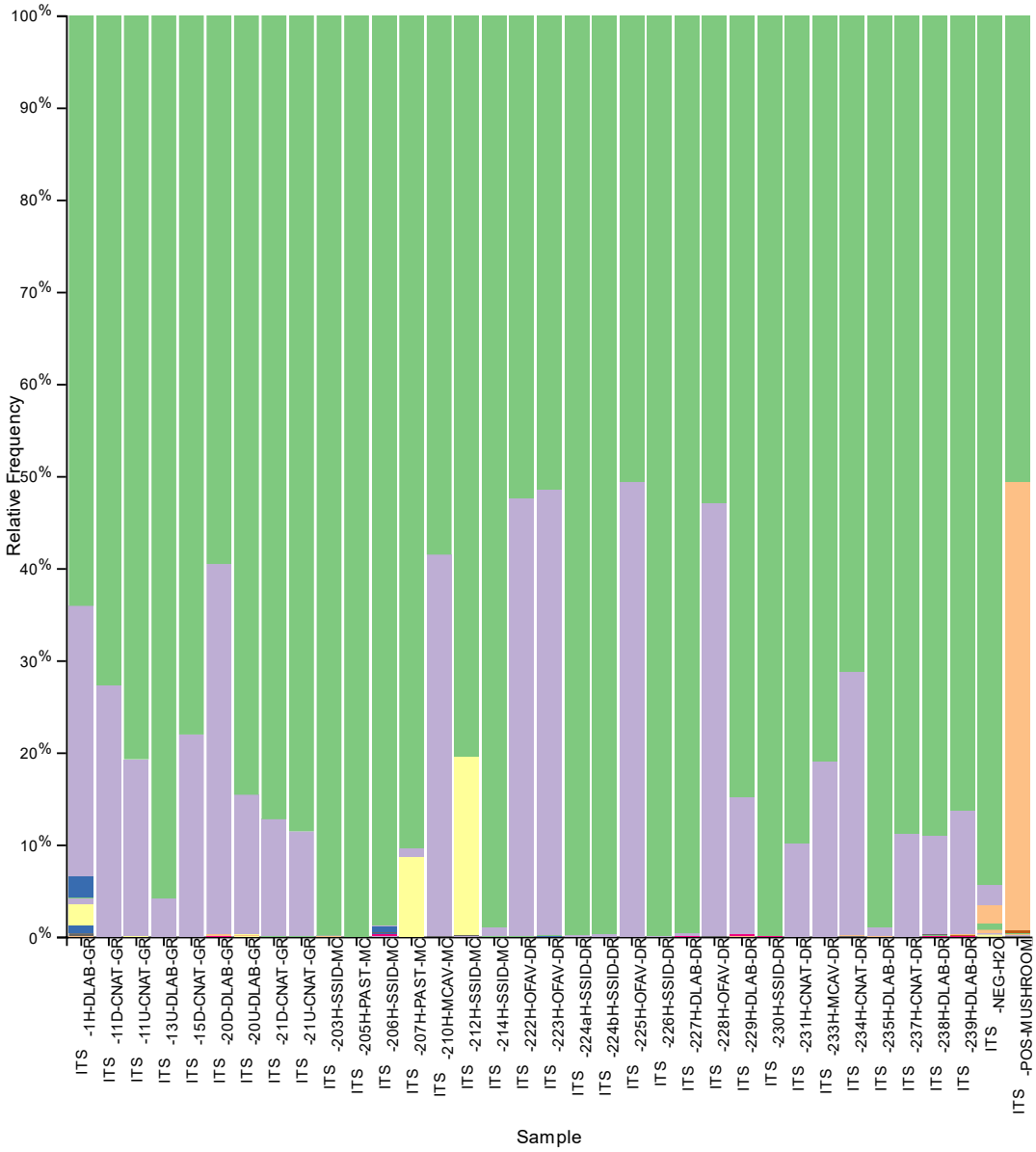

Figure 7: Taxonomic bar plot summary for ITS gene amplicon sequences (species level). The x-axis contains sample IDs: gene amplicon, sample number, health state (H = apparently healthy, U = unaffected, D = diseased, coral species, location collected). The y-axis is the relative abundance of different taxa in each sample. PCR positive and negative included for comparison. Color codes for all taxonomic groups are indicated in the legend on the following page (Table 8).

Table 8: Color codes for taxonomic groups in Figure 7

k__Fungi;__;__;__;__;__;__
k__Fungi;p__unidentified;c__unidentified;o__unidentified;f__unidentified;g__unidentified;s__unidentified
k__Fungi;p__Basidiomycota;c__Agaricomycetes;o__Agaricales;f__Psathyrellaceae;g__Coprinopsis;s__Coprinopsis_pachyderma
k__Fungi;p__Ascomycota;c__Dothideomycetes;o__Pleosporales;f__Didymellaceae;__;__
k__Fungi;p__Ascomycota;c__Dothideomycetes;o__Capnodiales;f__Cladosporiaceae;g__Cladosporium;s__Cladosporium_tenuissimum
k__Fungi;p__Ascomycota;c__Eurotiomycetes;o__Eurotiales;f__Aspergillaceae;g__Aspergillus;s__Aspergillus_pseudodeflectus
k__Fungi;p__Ascomycota;c__Sordariomycetes;o__Xylariales;f__Microdochiaceae;__;__
k__Fungi;p__Rozellomycota;c__unidentified;o__unidentified;f__unidentified;g__unidentified;s__unidentified
k__Fungi;p__Basidiomycota;c__unidentified;o__unidentified;f__unidentified;g__unidentified;s__unidentified
k__Fungi;p__Ascomycota;c__Dothideomycetes;o__Capnodiales;__;__;__
k__Fungi;p__Ascomycota;__;__;__;__;__
k__Fungi;p__Ascomycota;c__Dothideomycetes;o__Capnodiales;f__Cladosporiaceae;g__Cladosporium;s__Cladosporium_sphaerospermum
k__Fungi;p__Basidiomycota;c__Tremellomycetes;o__Tremellales;f__Rhynchogastremataceae;g__Papiliotrema;s__Papiliotrema_flavescens
k__Fungi;p__Ascomycota;c__Dothideomycetes;o__Pleosporales;f__Pleosporaceae;g__Alternaria;s__Alternaria_angustiovoidea
k__Fungi;p__Ascomycota;c__Dothideomycetes;o__Pleosporales;f__Sporormiaceae;g__Preussia;s__Preussia_flanaganii
k__Fungi;p__Ascomycota;c__Dothideomycetes;o__Dothideales;f__Dothioraceae;g__Dothiora;s__Dothiora_infuscans
k__Fungi;p__Ascomycota;c__Sordariomycetes;o__Xylariales;f__Microdochiaceae;g__Idriella;s__Idriella_lunata
k__Fungi;p__Ascomycota;c__Eurotiomycetes;o__Chaetothyriales;f__Herpotrichiellaceae;g__Exophiala;s__Exophiala_equina
k__Fungi;p__Ascomycota;c__Sordariomycetes;o__Xylariales;f__Bartaliniaceae;g__Bartalinia;s__Bartalinia_robillardoides
k__Fungi;p__Chytridiomycota;c__unidentified;o__unidentified;f__unidentified;g__unidentified;s__unidentified
k__Fungi;p__Basidiomycota;c__Agaricomycetes;o__Russulales;f__Stereaceae;g__Stereum;s__Stereum_hirsutum
k__Fungi;p__Ascomycota;c__Lecanoromycetes;__;__;__;__
k__Fungi;p__Basidiomycota;c__Agaricomycetes;o__Russulales;f__Stereaceae;g__Stereum;__
k__Fungi;p__Ascomycota;c__Lecanoromycetes;o__Pertusariales;f__Ochrolechiaceae;g__Ochrolechia;s__Ochrolechia_androgyna
k__Fungi;p__Basidiomycota;c__Malasseziomycetes;o__Malasseziales;f__Malasseziaceae;g__Malassezia;s__Malassezia_sympodialis
k__Fungi;p__Basidiomycota;__;__;__;__;__
k__Fungi;p__Ascomycota;c__Saccharomycetes;o__Saccharomycetales;f__Saccharomycetales_fam_Incertae_sedis;g__Candida;s__Candida_
k__Fungi;p__Ascomycota;c__Sordariomycetes;o__Diaporthales;f__Valsaceae;g__Cytospora;s__Cytospora_rhizophorae
k__Fungi;p__Basidiomycota;c__Agaricomycetes;o__Polyporales;f__Phanerochaetaceae;g__Bjerkandera;s__Bjerkandera_adusta
k__Fungi;p__Ascomycota;c__Dothideomycetes;o__Pleosporales;f__Didymellaceae;g__Didymella;__
k__Fungi;p__Ascomycota;c__Sordariomycetes;o__Xylariales;f__Sporocadaceae;g__Pestalotiopsis;s__Pestalotiopsis_rhododendri
k__Fungi;p__Ascomycota;c__Dothideomycetes;o__Pleosporales;f__Sporormiaceae;__;__
k__Fungi;p__Ascomycota;c__Dothideomycetes;o__Pleosporales;f__Longiostiolaceae;g__Crassiperidium;s__Crassiperidium_octosporum
k__Fungi;p__Chytridiomycota;__;__;__;__;__
k__Fungi;p__Basidiomycota;c__Malasseziomycetes;o__Malasseziales;f__Malasseziaceae;g__unidentified;s__unidentified
k__Fungi;p__Ascomycota;c__Pezizomycotina_cls_Incertae_sedis;o__Pezizomycotina_ord_Incertae_sedis;f__Pezizomycotina_fam_Incertae_se
k__Fungi;p__Ascomycota;c__Sordariomycetes;o__Xylariales;f__Bartaliniaceae;g__Bartalinia;s__Bartalinia_pondoensis
k__Fungi;p__Basidiomycota;c__Agaricomycetes;o__Auriculariales;f__Aporpiaceae;g__Elmerina;s__Elmerina_caryae
k__Fungi;p__Ascomycota;c__Sordariomycetes;o__Sordariales;f__Lasiosphaeriaceae;__;__
k__Fungi;p__Ascomycota;c__Dothideomycetes;o__Pleosporales;f__Didymellaceae;g__Epicoccum;s__Epicoccum_nigrum
k__Fungi;p__Ascomycota;c__Dothideomycetes;o__Pleosporales;f__Thyridariaceae;g__Parathyridaria;__
k__Fungi;p__Ascomycota;c__Sordariomycetes;o__Xylariales;f__Sporocadaceae;__;__
k__Fungi;p__Ascomycota;c__Dothideomycetes;o__Pleosporales;f__Pleosporaceae;g__Curvularia;s__Curvularia_pseudorobusta
k__Fungi;p__Ascomycota;c__Dothideomycetes;o__Pleosporales;f__Didymosphaeriaceae;g__Pseudopithomyces;s__Pseudopithomyces_rosa
k__Fungi;p__Ascomycota;c__Sordariomycetes;o__Hypocreales;f__Stachybotryaceae;__;__
k__Fungi;p__Ascomycota;c__Sordariomycetes;__;__;__;__
k__Fungi;p__Ascomycota;c__Sordariomycetes;o__Xylariales;f__Sporocadaceae;g__Pestalotiopsis;__
k__Fungi;p__Ascomycota;c__Dothideomycetes;o__Pleosporales;f__Phaeosphaeriaceae;g__Phaeosphaeria;s__Phaeosphaeria_poagena
k__Fungi;p__Ascomycota;c__Dothideomycetes;o__Pleosporales;f__Sporormiaceae;g__Preussia;s__Preussia_persica
k__Fungi;p__Basidiomycota;c__Malasseziomycetes;o__Malasseziales;f__Malasseziaceae;g__Malassezia;s__Malassezia_globosa
k__Fungi;p__Ascomycota;c__Sordariomycetes;o__Glomerellales;f__Glomerellaceae;g__Colletotrichum;s__Colletotrichum_anthrisci
k__Fungi;p__Basidiomycota;c__Tremellomycetes;o__Cystofilobasidiales;f__Mrakiaceae;g__Tausonia;s__Tausonia_pullulans
k__Fungi;p__Ascomycota;c__Dothideomycetes;o__Pleosporales;__;__;__
k__Fungi;p__Ascomycota;c__Dothideomycetes;o__Pleosporales;f__Phaeosphaeriaceae;g__Neosetophoma;s__Neosetophoma_rosigena
k__Fungi;p__Ascomycota;c__Dothideomycetes;__;__;__;__
k__Fungi;p__Basidiomycota;c__Tremellomycetes;o__Filobasidiales;f__Filobasidiaceae;g__Naganishia;s__Naganishia_cerealis
k__Fungi;p__Ascomycota;c__Sordariomycetes;o__Magnaporthales;f__Magnaporthaceae;g__Arxiella;s__unidentified
k__Fungi;p__Ascomycota;c__Sordariomycetes;o__Hypocreales;f__Nectriaceae;g__Fusarium;s__Fusarium_lacertarum
k__Fungi;p__Ascomycota;c__Sordariomycetes;o__Pleurotheciales;f__Pleurotheciaceae;__;__
k__Fungi;p__Ascomycota;c__Dothideomycetes;o__Pleosporales;f__Pleosporales_fam_Incertae_sedis;g__Pseudorobillarda;s__Pseudorobilla
k__Fungi;p__Basidiomycota;c__Agaricomycetes;o__Sebacinales;__;__;__
k__Fungi;p__Basidiomycota;c__Tremellomycetes;o__Filobasidiales;f__Filobasidiaceae;g__Naganishia;s__Naganishia_globosa

Table 9: Slide review summary

Species	Slide Number	Dominant Symbiont	H/L	General Condition Score*	LN Present in SBW
CNAT	20-030-1-1	Bl	H	3	
	20-037-1-1	B	H	4	
	20-043-4-1	B	H	4	Yes
	20-071-4-1	Bl	H	4	Yes
	20-073-2-1	B	H	5	
DLAB	20-046-3-1	NA	H	3	Yes
	20-058-2-1	D	H	4	Yes
MMEA	20-023-1-1	B	H	3	
	20-027-3-1	Bl	H	3	
	20-047-2-1	B	H	4	Yes
	20-065-1-1	B	H	4	
OFAV	20-050-1-1	Bl	H	5	Yes
	20-059-1-1	D	H	5	Yes
	20-100-3-1	C	L	5	**
	20-104-3-1	D	L	5	**
	20-111-2-1	Bl	L	5	**
PSTR	20-033-4-1	Bl	H	4	
	20-041-2-1	Bl	H	4	
	20-055-1-1	B	H	4	Yes
	20-068-3-1	B	H	4	Yes
	20-075-1-1	B	H	5	
	20-079-3-1	B	H	4	Yes

*0= Excellent, 1=Very Good, 2= Good, 3= Fair, 4= Poor, 5=Very Poor
**Abundant necrosis across entirety of tissue made it impossible to determine if lytic necrosis was present

as well as 59 of the apparently healthy samples. These signs can be indicative of poor overall health. As expected, this was seen microscopically as well. PSTR 20-068 (Figure 10) represents the condition of the majority of PSTR samples processed. Grossly, they had mild to moderate tissue rescission and algal overgrowth around their edges but also had collected mucus and debris between their ridges. The algal overgrowth is visible microscopically within the agarose as is some of the potential debris. Internally, endolithic fungi can also be seen surrounding areas of atrophied calicodermis.

In almost all cases, lesioned samples (L) were in worse condition than supposedly healthy (H) samples. Only three L samples were examined microscopically, all of which were OFAV. All three displayed gross signs of SCTLD as well as other signs of failing health, similar to what was described above. As seen in OFAV 20-104 (Figure 11), denuded skeleton around the septal ridges is apparent. Mesenteries have also been released in multiple polyps but are most numerous in those with denuded skeleton and those close to the algal overgrowth. Microscopically, the

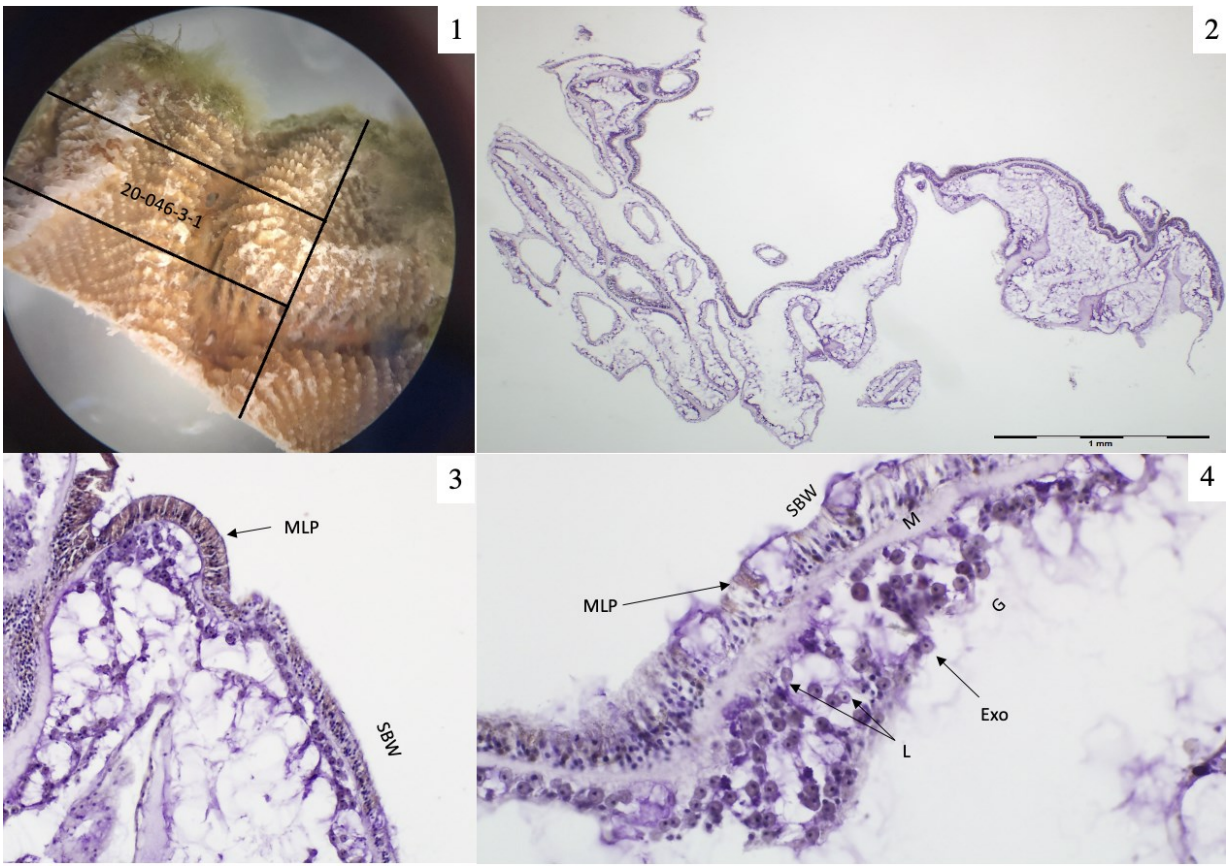

Figure 8: Gross and microscopic comparison of a half-core of *Diploria labyrinthiformis* collected after exposure of SCTLD but before appearance of gross lesions, symbiodinium species unknown. (1) Stereo photo taken at 1x magnification with histological section labeled; (2) DLAB 20-046-3-1, 10x. Alignment of ridges can be seen across gross photo and micrograph. Overall condition of tissue is poor with areas of lytic necrosis in the SBW and necrosis within the mesenteries and deeper tissue. (3) DLAB 20-046-3-1, 20x. Brown-staining melanin-like pigments (MLP) characteristic of the species visible in the SBW. (4) DLAB 20-046-3-1, 40x. Area of necrosis in gastrodermal tissue. Enlargement of the symbiosome with surrounding symbionts beginning to lyse (L) and exocytose (Exo) into the gastrovascular canal.

tissue's overall condition is ranked as very poor, with abundant necrosis, swollen mucocytes, excess mucus, as well as abundant algal overgrowth, endolithic fungi, and unidentified worm species. Interestingly, signs of LN are not apparent, but this may be due to the oblique cut of the section and the late stage of general necrosis.

All histoslides of *Meandrina meandrites* (MMEA) samples processed so far have come out in poor condition. As seen in Figure 12, both 20-023-1-1 and 20-027-3-1 were cut obliquely as compared to sagittally across the cnidoglandular bands. This was a re-occurrent problem both with MMEA samples, as well as half-core samples. Because of the delicate nature of the tissue after decalcification and how small the samples were, it was difficult to achieve sagittal sections using standard trimming techniques. Additionally, as seen in micrograph 6, abundant necrosis also made achieving a 'clean' histoslide difficult, as even with agarose, the poor condition of the

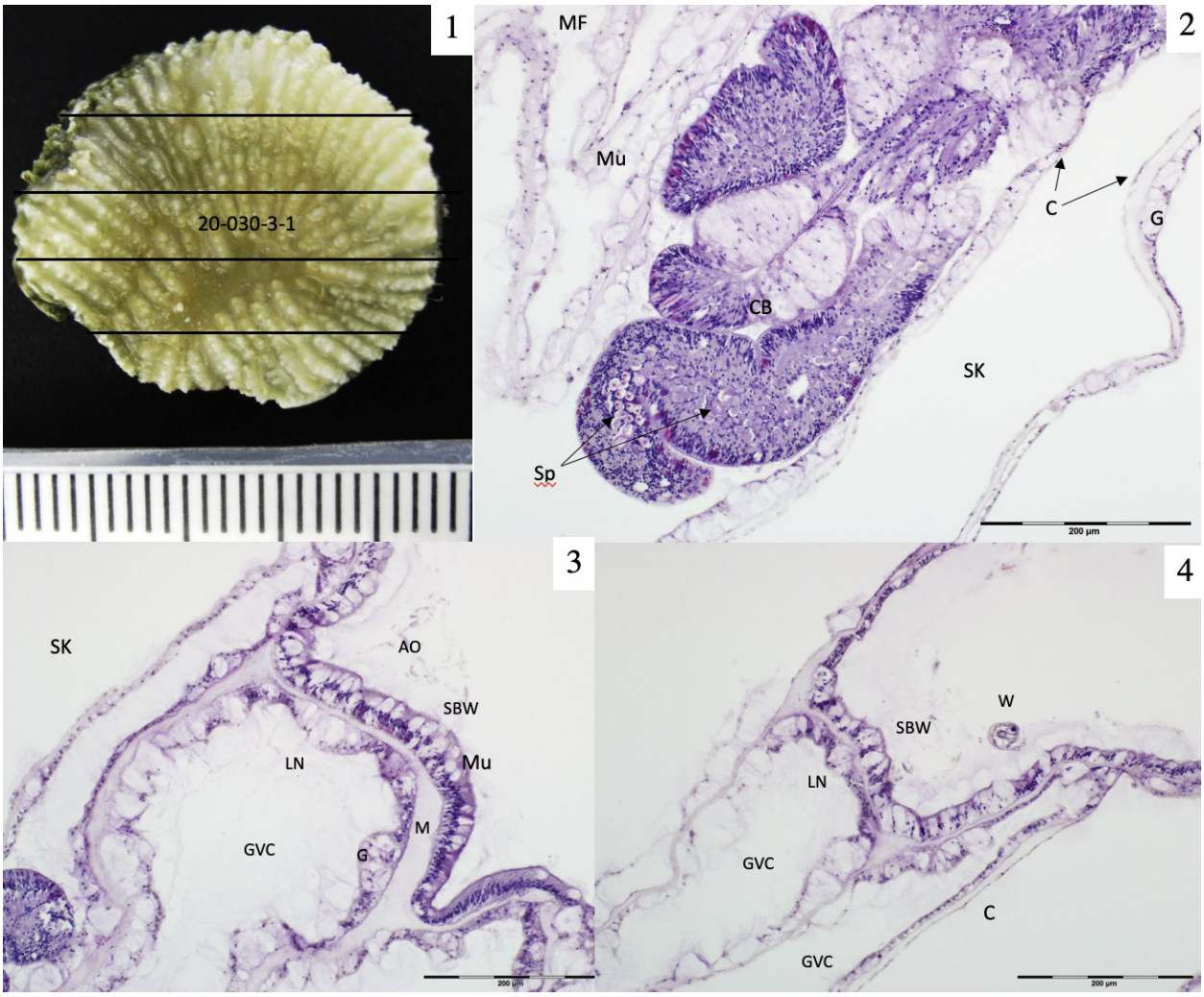

Figure 9: Gross and microscopic comparison of *Colpophyllia natans* collected after exposure to SCTLD but before appearance of gross lesions, bleached. (1) Gross photo of CNAT core with histological section labeled. (2) CNAT 20-30-3-1, 20x. Normal looking cnidoglandular band (CB) with numerous spirocysts and section through folds. Surrounding mesenterial filaments (MF) and mucocytes (Mu) can be seen to the left with calicodermis (C) and skeleton (SK) to the right. (3) CNAT 20-30-3-1, 20x. Area of lytic necrosis (LN) seen in gastrodermal tissue. Adjacent SBW also shows enlarged mucocytes with surrounding algal overgrowth within the agarose. Few to no symbionts in gastrodermis. (4) CNAT 20-30-3-1, 20x. Area of LN within the SBW. Enlarged mucocytes with debris and section through a worm in surrounding agarose.

tissue can cause disruptions that may be exacerbated by the trimming process. While this was a clear problem with MMEA, it also occurred in other corals that were in similar poor health. These results were presented to the Histopathology Subcommittee of the Research Team on the Disease Advisory Committee during their April 29, 2021, online meeting.

3.3. Task 3

3.3.1. Protocol Optimization Using Diseased and Healthy *A. cervicornis* As a Model Organism

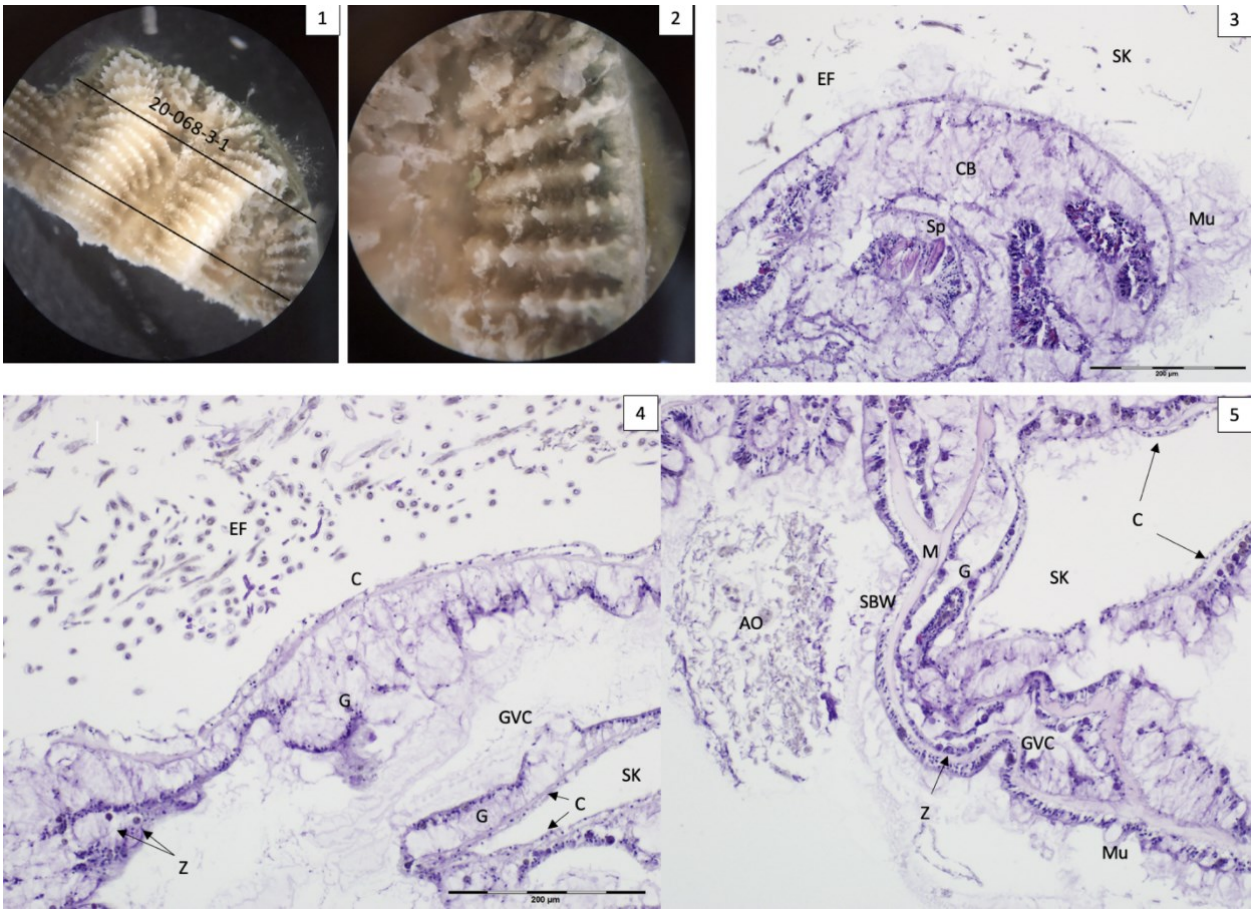

Figure 10: Gross and microscopic comparison of a half-core of *Pseudodiploria strigosa* collected after exposure of SCTLD but before appearance of gross lesions, symbiont species *Breviolum*. (1) Stereo photo taken at 1x magnification of PSTR 20-068 with histological section labeled. (2) Stereo photo taken at 3x magnification of PSTR 20-068. Tissue recession along edge and expanding onto septa. Algal overgrowth and accumulation of debris and mucus between ridges. (3) PSTR 20-068-3-1, 20x. Section of cnidoglandular bands shows abundant mucus being released within the band itself and into the surrounding area. Endolithic fungi are present within the surrounding skeleton. (4) PSTR 20-068-3-1, 20x. Calicodermis (C) beginning to detach from mesoglea with swollen mucocytes in adjacent gastrodermis (G) and endolithic fungi (EF) in adjacent skeleton (SK). Lytic necrosis seen in gastrodermal tissue in lower right corner of micrograph. (5) PSTR 20-068-3-1, 20x. Gastrodermal tissue (G) with few symbionts (Z) pulling away from mesoglea (M) with possible lytic necrosis. Algal overgrowth (AO) within agarose is adjacent to the surface body wall (SBW).

The manufacturer's protocol for the Apoptag Peroxidase In Situ Apoptosis Detection Kit is suitable for use on coral tissues with a few changes recommended for more accurate staining. Previous work examining the effect of blocking steps, proteinase K concentration, proteinase K incubation duration, epitope retrieval method, and counterstain type has improved the TUNEL protocol for use on FFPE coral tissues, however some samples processed with this adapted protocol continued to exhibit excessive background staining and unreliable stain quality that obscured morphological information and confounded results. The further optimization trials performed in this task on samples of *A. cervicornis* were able to further refine TUNEL staining

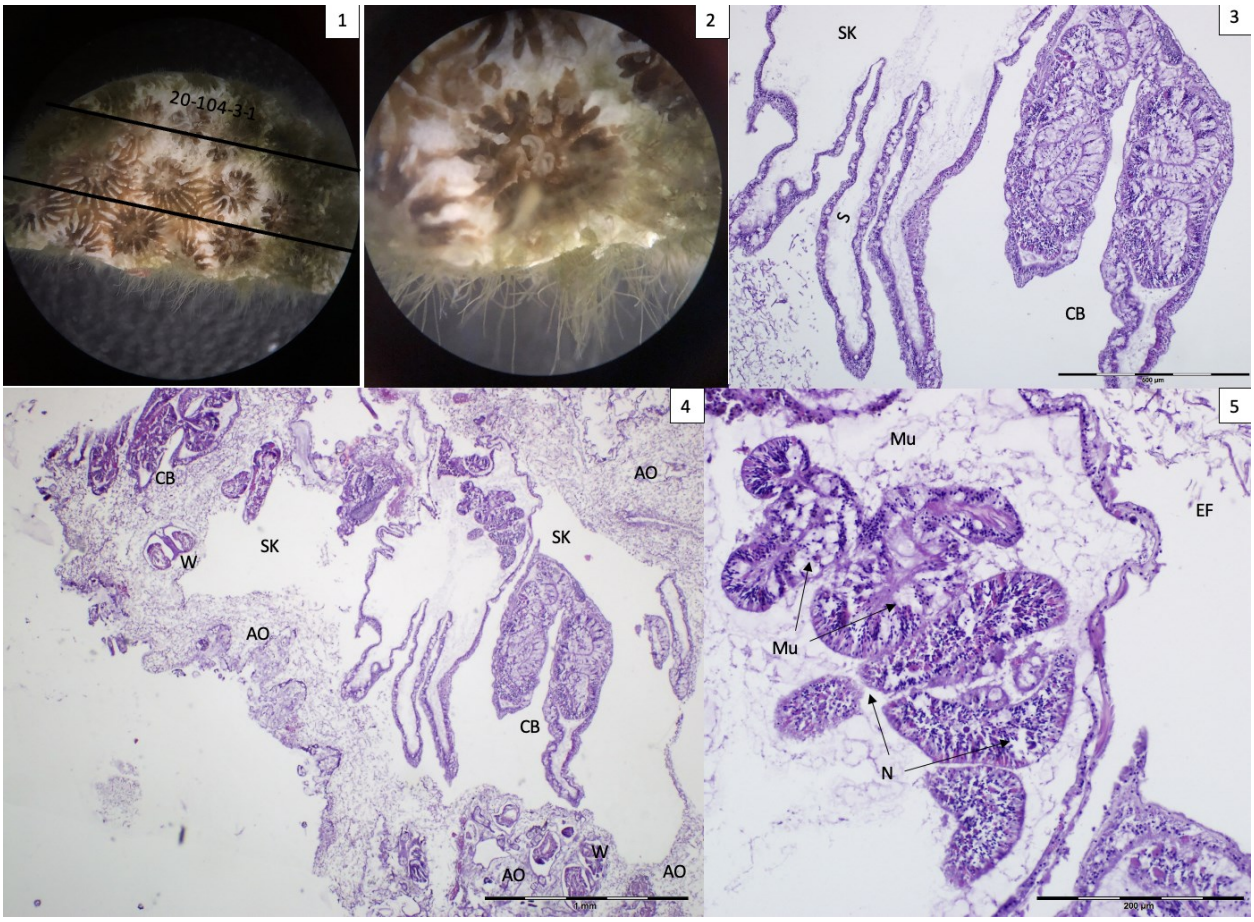

Figure 11: Gross and microscopic comparison of a half-core of *Orbicella faveolata* collected after gross signs of SCTLD appeared, dominant species *Durusdinium*.(1) Stereo photo taken at 1x magnification of OFAV 20-104 with histological section labeled. (2) Stereo photo taken at 3x magnification of OFAV 20-104. Mesenteries are released and denuded skeleton can be seen along septa. Algal overgrowth along the top and side of core is also present with surrounding tissue recession. (3) CNAT 20-104-3-1, 10x (incorrect scale bar). Section cut obliquely. Tissue along septa (S) is intact. Mild necrosis within cnidoglandular bands (CB) but relatively intact. (4) CNAT 20-104-3-1, 4x. Abundant algal overgrowth enrobed and within skeleton. Numerous parasitic organisms (W) can be seen adjacent to coral tissue. (5) Necrosis (N) and swollen mucocytes (Mu) within cnidoglandular bands. Excess mucus surrounds cnidoglandular bands.

technique on FFPE coral tissues to produce more consistent and reliable staining. To reduce the potential for false positive staining by chemically induced DNA fragmentation, samples fixed in Z-Fix (which contains zinc to prevent excessive crosslink formation during fixation), should be unmasked using a lower concentration of proteinase K (reduced from 20 µ g/mL to 5 µ g/mL) and the incubation duration reduced from 15 min to 5 min. Reducing this epitope retrieval step substantially reduced indiscriminate background staining with DAB peroxidase substrate in both *A. cervicornis* exhibiting tissue loss and in *P. strigosa* exhibiting SCTLD.

Reducing the incubation time with DAB peroxidase substrate from the recommended minimum of 1 min to ~30 s (the point at which the first indications of positive staining become visible in

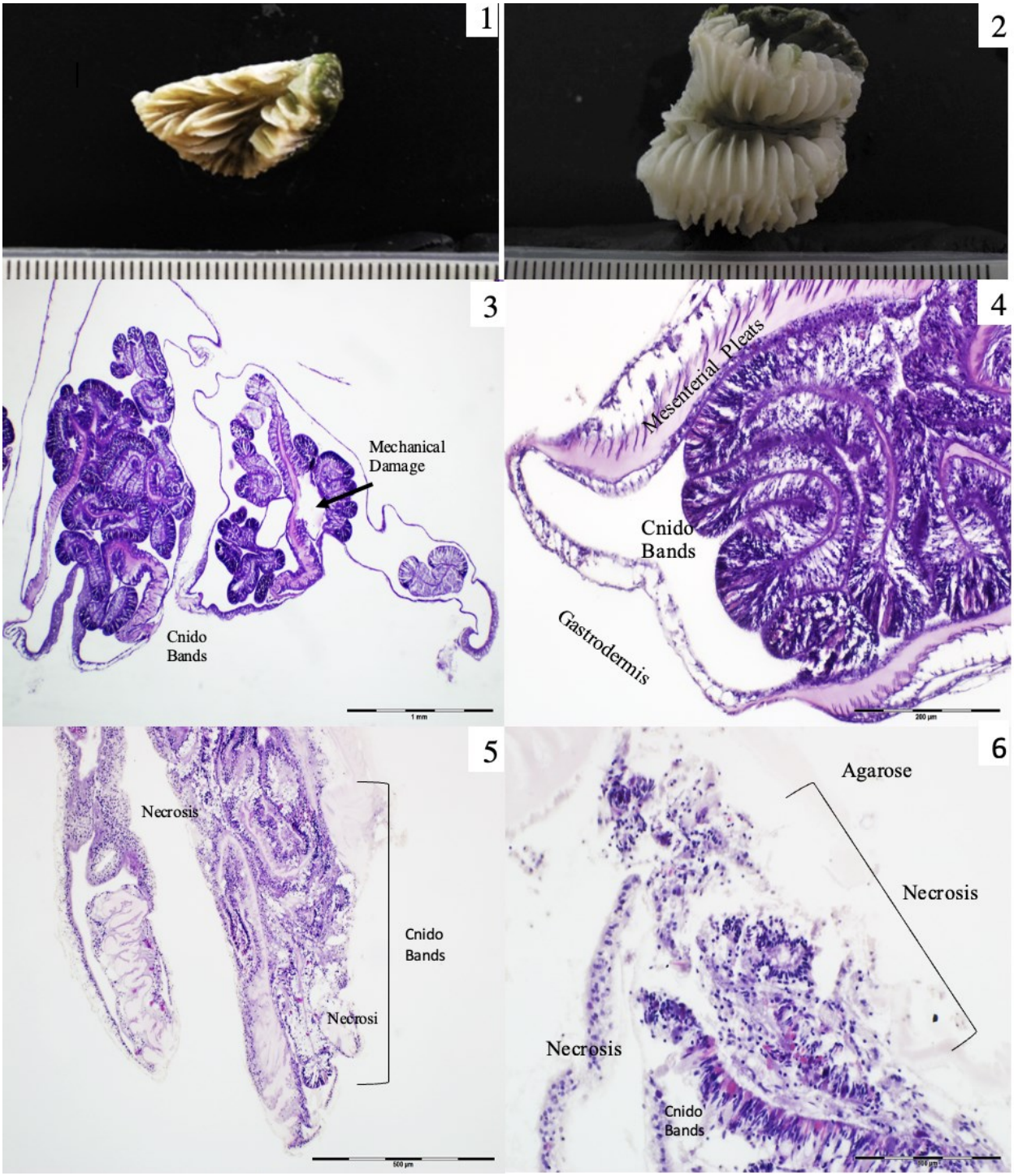

Figure 12: Gross and microscopic comparison of *Meandrina meandrites*, after exposure to SCTLD but no gross lesions. (1) Gross photo of 20-023, dominant species *Breviolum*. (2) Gross photo of 20-027, bleached. (3) MMEA 20-027-3-1, 4x. Mechanical damage from processing. (4) MMEA 20-027-3-1, 20x. Mild necrosis of cnido[glandular] bands, prominent mesogleal pleats. (5) 20-023-1-1, 10x. Necrotic cnidoglandular bands and mesenteries (N). (6) 20-023-1-1, 40x. Higher magnification of tissue from same coral as (5), agarose is present around the tissue.

diseased tissues) substantially reduced background staining while still effectively staining nuclei in *A. cervicornis* samples. When applying this change to samples of *P. strigosa*, *M. cavernosa*, and *O. faveolata*, ~30 s was consistently the time at which DAB first became visible and was found to produce the best stain quality.

Despite the improvements achieved by reducing proteinase K exposure and DAB substrate incubation, many samples continued to display some degree of cytoplasmic staining outside of target nuclei. However, this background staining was significantly more prevalent in diseased samples than in healthy samples (p=<0.0001, two-way ANOVA) and was not present in the negative control treatments where TdT enzyme was omitted in the staining protocol, indicating that his cytoplasmic staining is biologically relevant and may not be an inconsequential staining artifact. To test whether endogenous peroxidases in the coral tissues were inadequately quenched during the incubation step with H_2O_2 and were reacting with DAB substrate to produce this staining pattern, multiple incubation times (5 min, 15 min, 30 min) with H_2O_2 were tested with a fresh bottle of 30% H_2O_2 solution. The substantially improved staining quality evident in the higher incubation times indicates that this step should be extended to 30 min for use on FFPE coral tissues, and that excessive cytoplasmic staining in diseased corals may be caused by elevated peroxidases in the tissues.

3.3.2. Evidence for Apoptosis in SCTLD Pathology

Tissues from all tested samples displayed positive staining with the DAB peroxidase substrate indicating DNA fragmentation associated with apoptosis, including diseased, unaffected, and healthy tissues of *P. strigosa*, *M. cavernosa*, and *O. faveolata* (Figures 13). DAB-positive staining also appeared to be equally present in all tissue layers (epidermis, gastrodermis, calicodermis, and mesenteries) (Figure 14), but did appear to become more extensive in the deeper tissues of the polyp (Figure 15). There was significantly more DAB-positive staining in diseased tissues than in healthy tissues (p=<0.0001, Un-paired T-Test) (Figure 16), indicating that DNA fragmentation and apoptotic cell death may be involved in SCTLD pathology.

Positive DAB staining for apoptotic DNA fragmentation was present in all species tested, but the proportion of tissues stained with DAB versus hematoxylin was significantly higher in both the healthy and diseased tissues of *P. strigosa* than in *M. cavernosa* and *O. faveolata* (p=0.0041, Two-Way ANOVA) (Figure 17), with an average labelling index of 73% with a high background signal, compared to an average labelling index of 32% in *M. cavernosa* and 30% in *O. faveolata* (Table 10). Because a similar pattern of overstaining was consistent in all tissues of *P. strigosa*, including healthy tissue exhibiting no grossly detectable signs of disease, and because of the high degree of apparently indiscriminate staining of cytoplasmic material, this may have been the result of a faulty TUNEL reaction. It is still unclear why the *P. strigosa* samples appear to react so differently to the TUNEL protocol that has been shown to work effectively on *A. cervicornis*, *M. cavernosa*, and *O. faveolata*. In our previous work on developing these methods, one hypothesis for the problematic staining patterns in archived tissues of *P. strigosa* was that it might be caused by DNA damage resulting from extensive storage in fixative. This was proposed as a possibility due to the stark difference in stain quality between archived samples that were fixed for 100+ days and freshly collected samples which were fixed for ~1 week. However, the samples tested here of *M. cavernosa* and *O. faveolata* were fixed for a similar duration (100–300

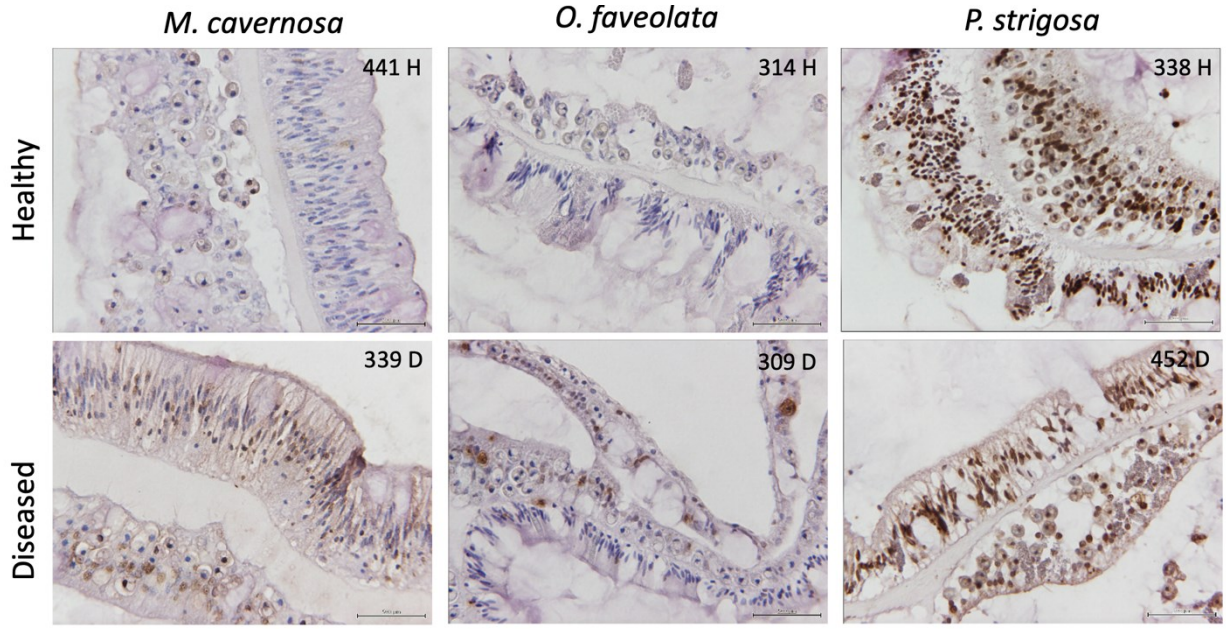

Figure 13: Micrographs showing the significantly higher DAB-positive staining in both diseased and healthy samples of *P. strigosa* than *M. caverno*sa and *O. faveolata*.

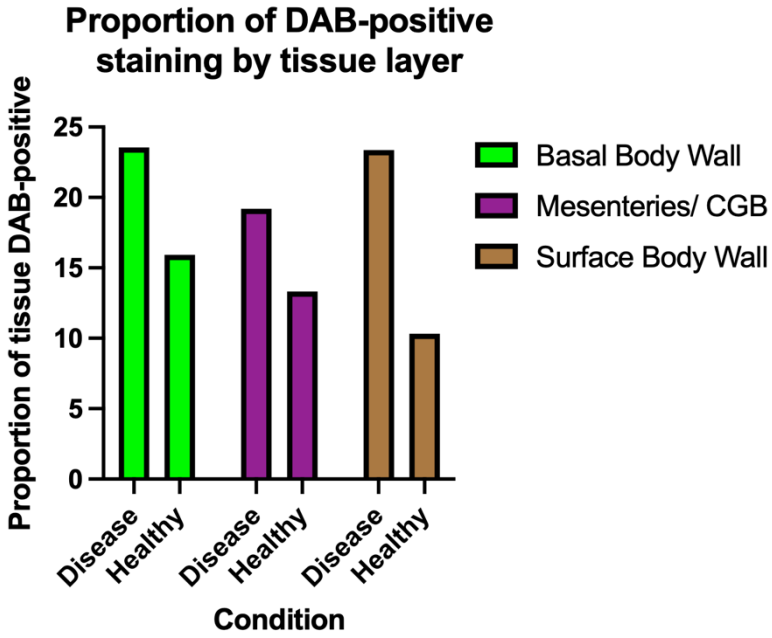

Figure 14: The proportion of tissue stained as DAB positive in the different tissue layers of both diseased and healthy tissue of *M. cavernosa* and *O. faveolata*. There is no significant difference in the degree of DAB-positive staining between the difference in the degree of DAB-positive staining between the different tissue layers (p=0.4794, Two-Way ANOVA).

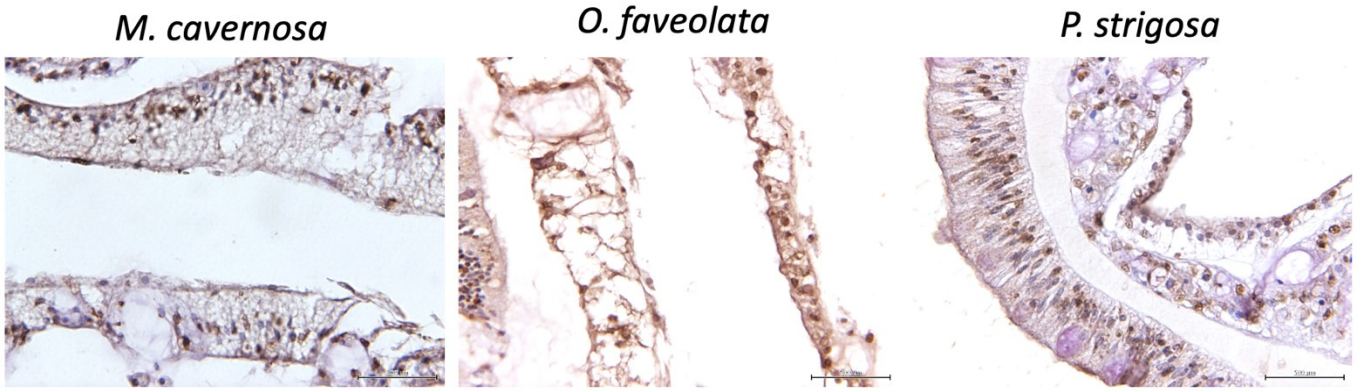

Figure 15: Example micrographs showing the high cytoplasmic staining with DAB-peroxidase substrate in the deep basal body wall diseased tissues of *M. cavernosa*, *O. faveolata*, and *P. strigosa*.

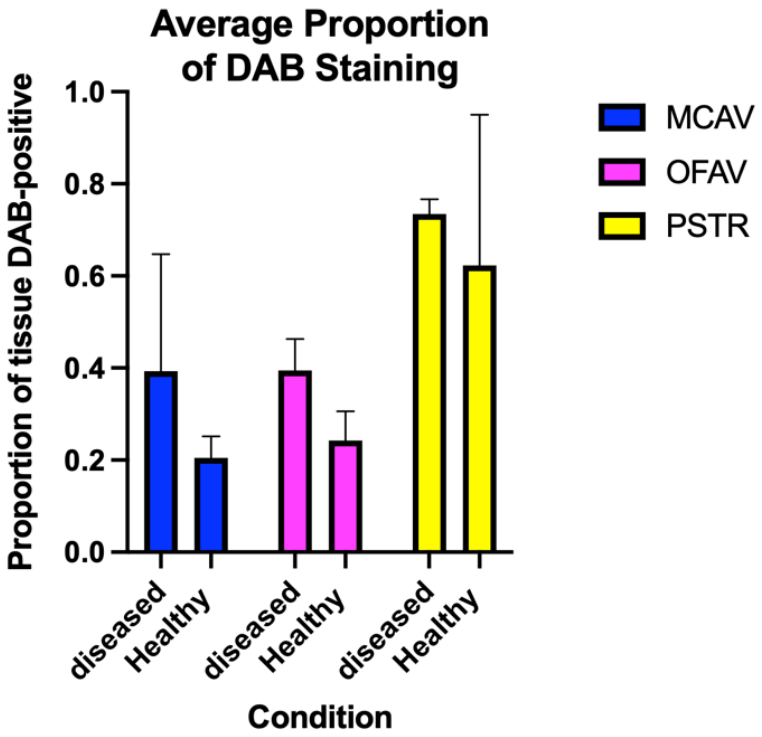

Figure 16: The proportion of tissue stained as DAB positive (indicating apoptosis) in the diseased and healthy tissue samples of *M. cavernosa*, *P. strigosa*, and *O. faveolata*. The proportion of DAB-positive tissue area was significantly higher in samples of *P. strigosa* (average 73%) than in both other species (average 32% and 30% for *M. cavernosa* and *O. f faveolata*, respectively) (p=0.0041, Two-Way ANOVA).

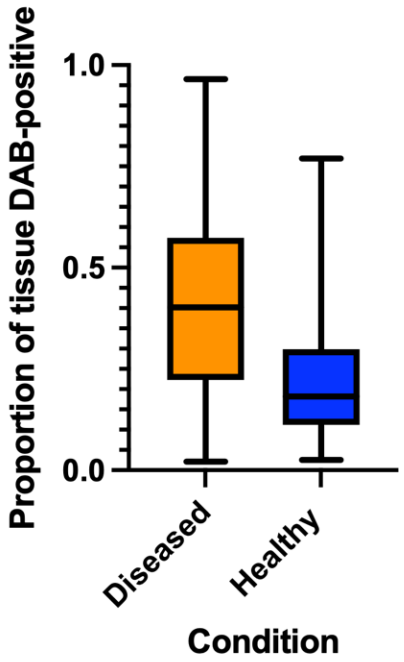

Figure 17: The proportion of tissue stained as DAB positive (indicating apoptosis) in the pooled diseased and healthy tissue samples of *M. cavernosa* and *O. faveolata*. The proportion of DAB-positive tissue is significantly higher in the diseased samples (average 41%) than in the healthy samples (average 32%) (p=<0.0001, Un-paired T-Test).

d) in the same solution and did not incur the same issues. Because the staining patterns observed in the *P. strigosa* samples were not indicative of genuine cellular processes, they were omitted from statistical analysis that produced the figures shown in this report. However, it is important to note that all statistical conclusions reached here do not change when the *P. strigosa* samples are included in the pooled datasets.

In all species, the proportion of DAB-stained tissues was significantly higher in diseased samples (p=<0.0001, Un-paired T-Test), indicating that apoptosis may be expressed in response to disease state and involved in SCTLD pathology. While the protocol modifications applied in this task did substantially improve the background staining of cytoplasmic material, some degree of indiscriminate staining did remain in the deeper tissue layers of diseased samples (Figure 14). Because of the clear difference in background staining prevalence in the different disease states, and because all DAB staining was removed in the negative control samples that were not exposed to TdT enzyme, we believe that this cytoplasmic staining is biologically relevant to SCTLD. There are a few possible explanations as to what the DAB substrate may be binding to in diseased tissues. First, there is some evidence that DAB can bind to calcium ions present in tissues, which can be remedied through additional calcium-chelating steps during processing, such as prolonged exposure to EDTA and modified epitope retrieval methods. Because the cytoplasmic staining is more prevalent in the deeper tissue layers of the calcifying polyps, it is possible that residual calcium in the polyp after the skeleton has been removed may be reacting to the DAB stain. However, because of the extensive exposure of FFPE coral samples to EDTA during the decalcification step of histological processing, and because multiple calcium-chelating processing steps were explored in previous work and did not improve background staining, we

Table 10: Average percentage of tissue stained with DAB in samples per species and condition

Sample ID	Percent (%) of tissue stained with DAB
Montastraea cavernosa	**32.06**
Diseased	**42.96**
319 D LS +	29.28
320 D LS -	68.60
399 D LS +	22.82
Healthy	**20.64**
321 H LS -	25.35
441 H LS +	16.07
482 H LS +	19.99
Orbicella faveolata	**30.51**
Diseased	**39.20**
308 D LS +	44.64
388 D LS +	42.02
390 D	31.80
Healthy	**23.97**
314 H LS +	16.97
435 H	28.66
475 H LS -	27.16
Pseudodiploria strigosa	**70.14**
Diseased	**73.39**
412 D	74.07
452 D	76.29
454 D	70.04
Healthy	**66.72**
338 H	29.55
417 H	94.95
457 H	62.35

find it unlikely that residual calcium is the cause of the cytoplasmic staining observed here. Future staining attempts with alizarin red stain, which binds to residual calcium, can be used to confirm this and determine the role of calcium ions in diseased SCTLD tissues. Another possible explanation for non-specific DAB staining may be that the endogenous peroxidases present in coral tissues were not adequately quenched in the incubation step with H_2O_2. By redoing the protocol using a fresh solution of 30% H_2O_2 and increasing the incubation time to 30 min, the cytoplasmic staining was substantially reduced (though not entirely alleviated), leading us to believe that an increased concentration of peroxidases in SCTLD tissues may be responsible for

the stain pattern observed here. Future work is needed to test this hypothesis and determine the role of peroxidase and oxidative stress in SCTLD.

Positive staining with DAB peroxidase substrate was present in all tissue layers (basal body wall, mesenteries, cnidoglandular bands, and surface body wall) (Figure 14). While the degree of DAB staining was not significantly different in in these tissue types (p=0.4794, Two-Way ANOVA), there did seem to be increased staining with polyp depth in all species. It is possible that this pattern indicates that SCTLD begins or is more severe deep in the coral polyp. However, it is also possible that this is indicative of patterns of normal cell turn over, and that tissues in the deeper polyp are more rapidly replaced. Future work is needed to determine the effect of tissue age and depth within the polyp in the tissue's reactivity to the TUNEL stain.

There was no relationship between the disease state and the presence of microlesions within the tissues (p=0.3343, Two-Way ANOVA). Ten of the eleven scored microlesion types were present in the diseased and healthy tissues of all species, the exception being mucocyte hypertrophy, which was not observed in any sample (Figures 18,19). While there was no significant difference between the pathology scores of the two conditions, it is interesting to note the high pathology score in the healthy tissue samples that were exhibiting no gross lesions. This demonstrates the importance of distinguishing between "apparently healthy" and "truly healthy" when describing samples and whole colonies in the field when histological information is not available. While all these tissues were grossly healthy, they were oftentimes rife with microscopic lesions that went

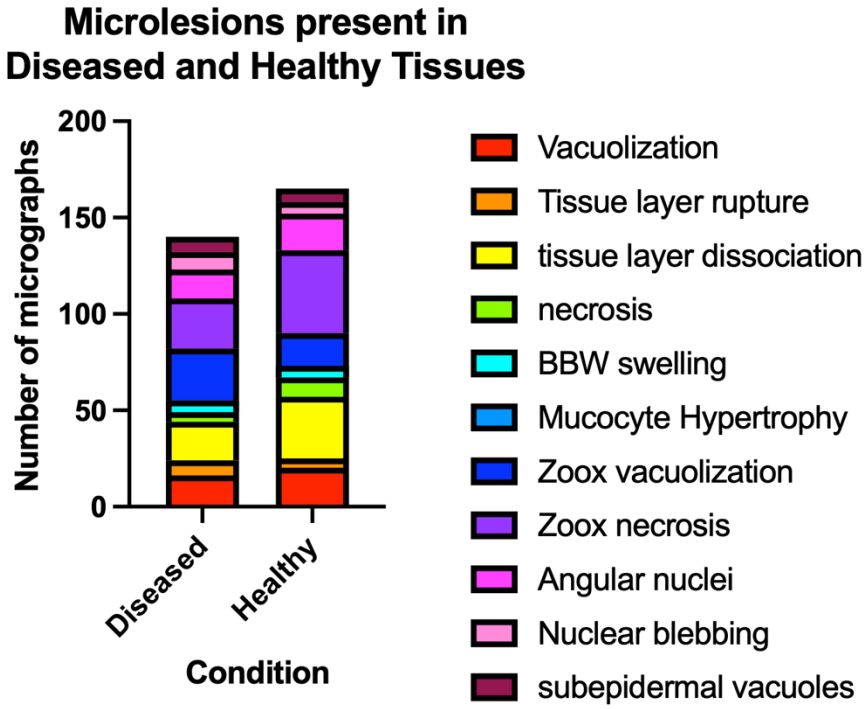

Figure 18: Microlesions present in photomicrographs of healthy and diseased tissues. There is no significant difference between the abundance of photomicrographs exhibiting any microlesion and the tissues condition (p=0.3343, Two-Way ANOVA).

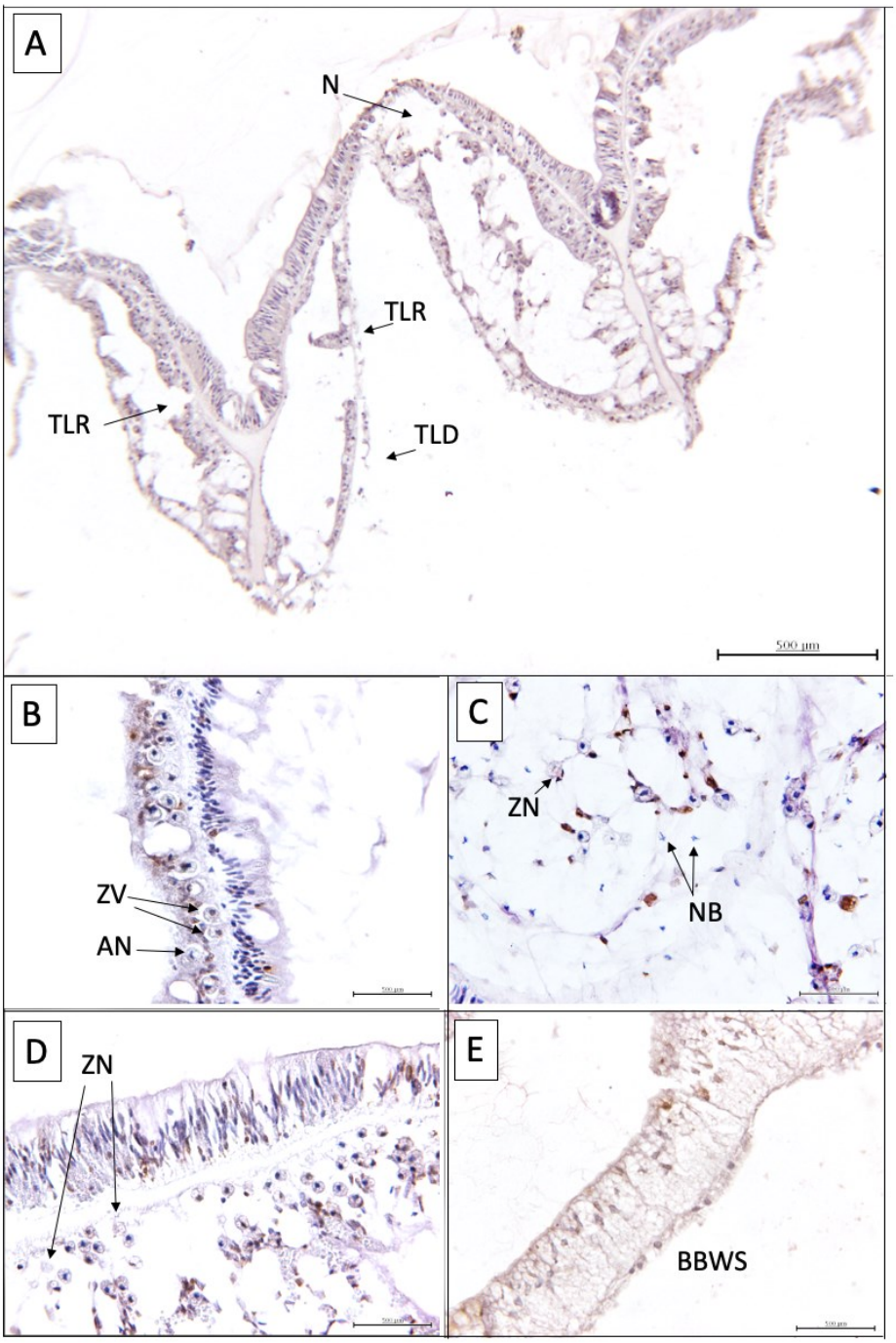

Figure 19: Micrographs of diseased *O. faveolata* exhibiting lesions: vacuolization (V), tissue layer rupture (TLR), tissue layer dissociation (TLD), necrosis (N), basal body wall swelling (BBWS), zooxanthellae vacuolization (ZV), zooxanthellae necrosis (ZN), angular nuclei in algal symbiont cells (AN), nuclear blebbing (NB) and subepidermal vacuoles (SV).
beyond what might be accepted as collection-related stress. Though each diseased and healthy sample did display some pathology, these scores do not reflect lesion severity, only the presence of absence of the lesion type. Further analysis of these micrographs will score the lesion severity

to determine if relationships between lesion severity, health state, and cell death activity become apparent.

These results were presented to the Histopathology Subcommittee on the Research Team of the Disease Advisory Committee during their March 5, 2021, online meeting.

3.4. Task 4

Three hundred histoslides were successfully scanned by an Aperio ScanScope slide scanner at 40x magnification. All digitized histoslide files were uploaded to Microsoft Azure cloud storage. The image files were linked to the developed filenames. FWC FWRI was able to find funding and is now purchasing Aperio's eSlideManager software to facilitate usage without downloading and the development of annotated slides and text.

4. DISCUSSION AND RECOMMENDATIONS

4.1. Task 1

Attempts to optimize the DNA extraction process for MCAV and other species through the addition of lysozyme and proteinase K to samples prior to extraction yielded mixed results for bacterial samples, but increased PCR yield for fungal analysis. **Preliminary results revealed differences in microbial (both bacterial and fungal) communities based on location and species, but not on health state—with the caveat that we had access to a limited number of diseased sample replicates.** A comparison of sequences generated from samples extracted using different methods will be completed to assess effects of extraction technique on taxonomic information yielded and to determine if these datasets can be combined to increase sample replicates for analysis. Several dominant bacterial phylotypes were present across all samples, and a few taxonomic groups found in diseased corals from other studies (e.g., Clostridia, Rhizobiales, Vibrios) were also identified in a single diseased CNAT sample and in unaffected tissues from four diseased colonies examined in this study (Meyer et al. 2019; Rosales et al. 2020). Further analysis with additional replicates needs to be completed to determine the significance of this finding. Fungal samples were dominated by unassigned reads at the Kingdom Fungi level. Further optimization of the bioinformatic pipeline will be conducted to resolve unassigned reads as done for bacterial samples to provide taxonomic identification for these sequences. Additional analyses will be conducted on metagenomic sequences to examine functional potential of the endolithic coral microbiome.

Management recommendations: Bacterial, archaeal, and fungal microorganisms present indicate that additional sequencing and analyses must be conducted to better understand their roles in apparently healthy and SCTLD-affected corals. Antibiotic treatments being used may adversely affect microorganisms that are necessary for optimum coral health and more targeted antimicrobials might be optimal, both for corals in the field and corals rescued and held in aquaria. Altered microhabitat conditions (e.g., temperature, pollutants) may support pathogenic microorganisms; perhaps some reefs will be spared if those microorganisms and conditions can be identified. Molecular analyses of the endolithic communities, obtained by crushing the tissue remaining deep in the skeleton as well as the skeleton as in the method used here, need to be

interpreted in conjunction with histopathology to better understand the specificity of these associations and potential roles in coral host health.

4.2. Task 2

Results from Task 2 were presented to the Histopathology Core Group of the Disease Advisory Committee on Microscopy analysis of the 2016 FWRI slides showed abundant necrosis and degradation of algal cells within apparently healthy, diseased, and unaffected samples. Comparing diseased and unaffected slides from the same colony did not give any indication as to which, if any, pathological sign was the first to appear. Similarly, both healthy and lesion slides collected by Dr. Baker's lab also showed abundant necrosis and degradation throughout the tissue. As both types of samples were collected after exposure to SCTLD, characteristics of the disease were expected to be seen within both subgroups. In almost all cases, multiple forms of necrosis and degradation were present on each photomicrograph. Vacuolation was most common, with severity corresponding with algal condition. Areas with severe vacuolation often had swollen or lysing algal cells as well, indicating the symbiosome has some effect in pathology. Of the six bleached samples analyzed, two displayed lytic necrosis in the surface body wall despite lacking symbionts. This possibly suggests that the pathology may begin in the coral tissue. Further analysis with a larger sample size will need to be examined to further support this conclusion.

During the processing of the Baker samples, additional questions beyond the role of symbionts in the pathology of SCTLD arose. Extended time was taken to document the gross condition of each sample with gross and stereo photos. Eighty-two of the 92 samples provided needed to be enrobed because they displayed signs of poor health including denuded skeleton, tissue recession, algal overgrowth, and extended mesenteries. While all samples were collected post-SCTLD exposure, and some did show gross signs of the disease, many seemed to have additional health issues. Algal overgrowth, referring to when algae had begun to encroach on living coral tissue, was abundant on many of the samples. This resulted in tissue recession in the surrounding areas and extended mesenteries within adjacent polyps. This was also reflected in the histoslides where algae trapped in agarose could be seen adjacent to both healthy and affected coral tissue. Worms and endolithic fungi were also seen in the underlying skeleton of many samples. While this typically would not cause issue, there were indications that it was affecting nearby tissue, such as atrophying calicodermis, necrosis of adjacent cnidoglandular bands, and excessive mucus.

Difficulties were also faced during sample processing with MMEA samples. The fragility of their large polyps makes the species difficult to work with even under ideal circumstances, such as field collection. These cored aquaria samples consisted of a single manipulated polyp. Despite taking precautions by enrobing the majority of MMEA samples, after decalcification the tissue was so fragile that trimming the sections often resulted in awkwardly cut sections and mechanical tearing, as evidenced in the histoslides. This problem also extended to half-cores of other species. The compounding issues of poor overall condition and small samples again resulted in awkwardly cut sections as well as subsamples that were too small to provide sufficient data. While this could potentially be rectified with practice processing such samples,

moving forward, using core samples less than 2.5 cm in diameter for histopathology is not recommended.

Research for Task 2 is ongoing as the Baker samples are still being processed. Once all histoslides are created, further conclusions can be drawn about the role of symbionts in SCTLD. By creating a spatial awareness of what is occurring within the tissue itself, a better overall understanding of the disease is more likely. Comparing both the FWRI and Baker samples will help create a foundation for understanding the relationship that dinoflagellates have with SCTLD. Describing the differences in tissue condition between opportunistically collected corals and aquaria corals will also likely provide insights on the effects that aquaria can have when conducting transmission studies.

Management recommendations: Histological observation needs to become the standard in aquaria trials testing different exposure parameters. While data are sparse in the literature, corals react differently in in-situ and ex-situ environments. Larger biopsy cores or fragments need to be used after a period of healing to provide more polyps and tissue that are not compromised by damage or fouling on their margins during the experiments. Not even describing the potential changes in their holobionts, general health due to aquaria conditions needs to be considered when describing the outcome of any experimental design. Specifically with transmission trials, exposing a compromised coral to disease is not informative. Ensuing signs cannot be attributed specifically to a single disease if a coral is already sick. Histopathology needs to be used in conjunction with molecular techniques both to support findings and as a quality check.

4.3. Task 3

Positive staining with the TUNEL method, which indicates the presence of DNA fragmentation associated with apoptosis, was consistently observed in the tissues of *P. strigosa*, *M. cavernosa*, and *O. faveolata* affected by SCTLD, suggesting that this mode of cell death is involved in SCTLD pathology. DNA fragmentation was also detected in all healthy samples to a lesser degree, indicating either that this process is a highly expressed part of routine cell turn over or coral physiology, or that it is an early clinical sign of stress or disease that can be detected before gross lesions form. Determining which of these scenarios is more likely is not possible with the data acquired in this task, particularly with the state of the apparently healthy tissues collected here being microscopically compromised. Future work is needed to determine the routine expression of apoptosis and DNA fragmentation in truly healthy and apparently healthy coral tissues to better understand how often corals rely on this immune pathway, and how it might become dysregulated during times of stress and disease.

In many of the diseased coral tissues, the TUNEL stain produced an abnormally high degree of cytoplasmic staining that in some cases was severe enough to obscure the nuclei that were the target of this investigation. It is not possible to determine the cause of this staining pattern with the available data, however, the positive effect of increasing the incubation period in a fresh solution of H_2O_2 suggests that a high concentration of peroxidase may be reacting to the DAB peroxidase substrate. The spatial pattern of excessive cytoplasmic staining in the deepest layers of the polyp suggest a concentration of potential oxidative damage in this area, which has interesting implications for the beginning of SCTLD, coral physiology, and tissue age in

reponses to stress. Excessive peroxidase levels in tissues are associated with a variety of known diseases and can be a marker of oxidative damage in cells. Determining whether elevated peroxidases and oxidative damage are involved in SCTLD pathology in future work will provide valuable information as to the earliest stages of SCTLD pathogenesis.

There was no significant difference in the abundance of microlesions in either the healthy or diseased tissue conditions of all species, demonstrating how prevalent these indicators of stress and disease were in the apparently healthy samples. Lesions were just as common in apparently healthy tissues with a low DAB signal as in diseased and apparently healthy samples with a higher DAB signal, indicating that the presence of these lesions and the cause of DAB staining (DNA fragmentation, elevated peroxidases) are independent of one another. A deeper analysis will include parameters that better reflect the lesion severity, rather than the binary presence/absence approach taken here. However, the sheer abundance of lesions in healthy samples has important implications for our understanding of "apparently healthy" tissues, and our interpretation of diseases versus collection-related stress or artifacts produced in processing.

Management recommendations: Because positive staining for apoptosis was highly prevalent in SCTLD-afflicted corals, this process is expressed in response to this disease and may provide important information for the pathogenesis of SCTLD. Preliminary analysis suggests that the expression of apoptosis was independent of the presence of microlesions associated with SCTLD and general cellular stress. This information furthers our understanding of cell death mechanisms in scleractinian corals and provides preliminary work to support future studies into both routine and pathological cell death mechanisms and the use of immunohistochemistry in corals. This tool should be included in coral disease laboratory diagnosis tests to complement histopathological examinations and molecular microbiological analyses to improve our ability to identify the pathogen(s) responsible for SCTLD.

4.4. Task 4

The outcomes of Task 4 will provide the functionality required for investigators from different places to virtually collaborate on histology slide work without Convention on International Trade in Endangered Species (CITES) permits. It will also eliminate the need to prepare and ship multiple serial sections from tissue blocks. This group now has more than 10 veterinary and invertebrate histopathologists and their students, from academia and federal/state agencies, who are studying SCTLD in Florida or Caribbean sites. Besides being a data repository for selected samples, the digital images will improve our investigations on etiologic agents and mechanisms of pathogenesis, as well as for comparisons with other studies and collaboration on case descriptions. Histopathologists will be able to view tissue sections on a computer as if a microscope were being used. Aperio ImageScope will allow investigators to consult with others for diagnostic quality assurance, annotate histoslides, and provide educational resources to those studying coral disease. Collaboration between investigators will improve investigations on etiologic agents and mechanisms of pathogenesis and facilitate comparisons with other studies and collaboration on case descriptions.

Management recommendations: The electronic histoslides archive allows investigators to retain important data and observations indefinitely and collaborate at national and international levels.

The methods used to develop this program may be applied beyond the scope of SCTLD research. Continuing archive support will help train more histopathologists to improve disease diagnosis.

5. LITERATURE CITED

Apprill, A., McNally, S., Parsons, R., & Weber, L. (2015). Minor revision to V4 region SSU rRNA 806R gene primer greatly increases detection of SAR11 bacterioplankton. Aquatic Microbial Ecology, 75. https://doi.org/10.3354/ame01753

Callahan, B. J., McMurdie, P. J., & Holmes, S. P. (2017). Exact sequence variants should replace operational taxonomic units in marker-gene data analysis. The ISME Journal, 11(12), 2639–2643. https://doi.org/10.1038/ismej.2017.119

Callahan, B. J., McMurdie, P. J., Rosen, M. J., Han, A. W., Johnson, A. J. A., & Holmes, S. P. (2016). DADA2: High-resolution sample inference from Illumina amplicon data. Nature Methods, 13(7), 581–583. https://doi.org/10.1038/nmeth.3869

Clode, P. L., Saunders, M., Maker, G., Ludwig, M., & Atkins, C. A. (2009). Uric acid deposits in symbiotic marine algae. Plant, Cell & Environment, 32(2). https://doi.org/10.1111/j.1365-3040.2008.01909.x

Gardes, M., and Bruns, T. D. (1993). ITS primers with enhanced specificity for basidiomycetes-application to the identification of mycorrhizae and rusts. Molecular Ecology 2(2), 113–118.

Green, D. (2011). Means to an End: Apoptosis and Other Cell Death Mechanisms. Cold Spring Harbor Laboratory Press, Maine.

Katoh, K., Misawa, K., Kuma, K., & Miyata, T. (2002). MAFFT: A novel method for rapid multiple sequence alignment based on fast Fourier transform. Nucleic Acids Research, 30(14), 3059–3066.

Landsberg, J. H., Kiryu, Y., Peters, E. C., Wilson, P. W., Perry, N., Waters, Y., Maxwell, K. E., Huebner, L. K., and Work, T. M. (2020) Stony coral tissue loss disease in Florida is associated with disruption of host–zooxanthellae physiology. Frontiers in Marine Science. 7:576013. https://doi.org/10.3389/fmars.2020.576013

Meyer, J. L., Castellanos-Gell, J., Aeby, G. S., Häse, C. C., Ushijima, B., & Paul, V. J. (2019). Microbial Community Shifts Associated With the Ongoing Stony Coral Tissue Loss Disease Outbreak on the Florida Reef Tract. *Frontiers in Microbiology*, *10*. https://doi.org/10.3389/fmicb.2019.02244

Parada, A. E., Needham, D. M., & Fuhrman, J. A. (2016). Every base matters: Assessing small subunit rRNA primers for marine microbiomes with mock communities, time series and global field samples. Environmental Microbiology, 18(5), 1403–1414. https://doi.org/10.1111/1462-2920.13023

Precht, W. F., Gintert, B. E., Robbart, M. L., Fura, R., & van Woesik, R. (2016). Unprecedented disease-related coral mortality in southeastern Florida. Scientific Reports 6, 31374, https://doi.org/10.1038/srep31374

Price, K. L. & Peters, E.C. (2018). Histological Techniques for Corals. Published by Kathy L. Price, Glen Muir Technologies, and Esther C. Peters, Pathobiology Consulting Services.

Rasband, W. S. (2020). ImageJ, U. S. National Institutes of Health, Bethesda, Maryland, USA, https://imagej.nih.gov/ij/, 1997-2018

Rosales, S. M., Clark, A. S., Huebner, L. K., Ruzicka, R. R., & Muller, E. M. (2020). Rhodobacterales and Rhizobiales Are Associated With Stony Coral Tissue Loss Disease and Its Suspected Sources of Transmission. *Frontiers in Microbiology*, *11*. https://doi.org/10.3389/fmicb.2020.00681

Salerno, J. L., & Peters, E. C. (2020). Microscopic and Microbial Insights into the Stony Coral Tissue Loss Disease (SCTLD) Outbreak Across Multiple Coral Species on Florida's Coral Reef. Florida DEP. Miami, FL. Pp. 42.

Walton, C. J., Hayes, N. K., & Gilliam, D. S. (2018). Impacts of a regional, multi-year, multi-species coral disease outbreak in Southeast Florida. Frontiers in Marine Science, 5. https://doi.org/10.3389/fmars.2018.00323

White, T. J., Bruns, T., Lee, S. J. W. T., and Taylor, J. L. (1990). Amplification and direct sequencing of fungal ribosomal RNA genes for phylogenetics. PCR Protocols: A Guide to Methods and Applications, 18(1), 315-322.